JAIST Repository
https://dspace.jaist.ac.jp/

| | |
|---|---|
| Title | Ternary mixing: A simple method to tailor the morphology of organic solar cells |
| Author(s) | Campoy-Quiles, Mariano; Kanai, Yoshihiro; El-Basaty, Ahmed; Sakai, Heisuke; Murata, Hideyuki |
| Citation | Organic Electronics, 10(6): 1120-1132 |
| Issue Date | 2009-06-08 |
| Type | Journal Article |
| Text version | author |
| URL | http://hdl.handle.net/10119/9197 |
| Rights | NOTICE: This is the author's version of a work accepted for publication by Elsevier. Mariano Campoy-Quiles, Yoshihiro Kanai, Ahmed El-Basaty, Heisuke Sakai,and Hideyuki Murata, Organic Electronics, 10(6), 2009, 1120-1132, http://dx.doi.org/10.1016/j.orgel.2009.05.028 |
| Description | |

JAIST
JAPAN
ADVANCED INSTITUTE OF
SCIENCE AND TECHNOLOGY

Japan Advanced Institute of Science and Technology

*Organic Electronics*, **10,** 1120-1132 (2009)

# Ternary mixing: a simple method to tailor the morphology of organic solar cells

Mariano Campoy-Quiles[1, 2, *], Yoshihiro Kanai[1], Ahmed El-Basaty[1], Heisuke Sakai[1] and Hideyuki Murata[1]

[1] School of Material Science, Japan Advanced Institute of Science and Technology (JAIST), Asahidai 1-1, Nomi, Ishikawa 923-1292, Japan.
[2] Institut de Ciència de Materials de Barcelona (ICMAB-CSIC), Campus de la Universitat Autònoma de Barcelona, 08193, Bellaterra, Spain.

*Corresponding author: Dr. M. Campoy-Quiles
Telephone: +34 935 801 853 (ext 292); Fax: +34 935 805 729
e-mail: mariano.campoy@icmab.es
Other authors emails: Prof. H. Murata: murata-h@jaist.ac.jp; Mr. H. Sakai: hsakai@jaist.ac.jp; Mr. A. El-Basaty: ahmedbakr@jaist.ac.jp; Mr. Y. Kanai: s0730021@jaist.ac.jp

**Abstract**

We present a detailed study of the effects of ternary mixing on blend morphology, charge carrier mobility and organic solar cell performance. We investigate ternaries consisting of regio random poly(3-hexylthiophene) (P3HT), regio regular P3HT and soluble fullerene derivative, PCBM. By means of absorption, photoluminescence, atomic force microscopy and X-ray diffraction, we demonstrate that the structure of ternary films consists of crystallites of regular P3HT embedded into a random polymer matrix acting as a soft scaffolding where PCBM can only form nanoscale aggregates but cannot grow the detrimental micron size structures often observed in the conventional regular P3HT:PCBM case upon annealing. The ternary films exhibit higher degree of crystallinity than the conventional blends, but with smaller crystallite sizes. Moreover, we show that the addition of the random polymer chains does not prevent good charge

carrier transport for regio random P3HT concentrations up to 50% of the total polymer content. Finally, we prove that solar cells based on the ternary systems have a similar short circuit current than the conventional binary, but improved open circuit current (by ~100 mV), which leads to an overall enhancement of power conversion efficiency.

**Keywords**: Polymer:fullerene solar cells, ternary systems, bulk heterojunction, morphology, transport, Polythiophene.

**PACS codes**: 68.55.am, 81.40.Rs, 81.40.Tv, 82.35.Cd, 84.60.Jt, 85.60.Dw

## 1 Introduction

The emergence of organic solar cells has been facilitated by cell design concepts that are radically different from the inorganic planar single heterojunction solar cells in production today [1]. The basis of these concepts is the existence of nanosized domains resulting in a bulk-distributed interface and thus the name of bulk heterojunction solar cells. In organic semiconductors, absorption of light leads to room temperature bound electron-hole pairs (c.f. free carriers in their inorganic counterparts). Excitons dissociate into free carriers mainly at the distributed interface, thus a large interface in organic photovoltaic (OPV) devices is needed to maximize charge generation. Upon exciton splitting, the photogenerated carriers travel through appropriate percolating pathways until they are collected at the contacts. The synthesis of novel materials, combined with good control of the morphology of the active layer and optimized device design has lead to a substantial progress in the field, with the best power conversion efficiencies achieved in the laboratory currently being in the 5-6% range [1-3].

For a given material system, the control of the blend structure at the nanoscale is, in fact, one of the most effective ways to significantly enhance the organic solar cell efficiency. In the case of the most extensively studied material systems (e.g. poly(3-hexylthiophene) (P3HT) and soluble fullerene derivative PCBM), ten fold increases in the power conversion efficiency have been reported when comparing devices based on as-spun active layers, and active layers with a controlled structure [4]. Typical protocols include slow drying of the active layer, thermal and vapor annealing, as well as appropriate solvent (or solvent mixture) choices [4-8]. A comprehensive review on the effect that morphology has on bulk heterojunction solar cells has been recently published by Yang and Loos [9]. Interestingly, it has been found that for the case of P3HT:PCBM blends, all of these fabrication protocols result in a similar optimized morphology (see Ref. [8] and references therein). This consists of a bicontinuous blend of the electron donor (the polymer chains) and electron acceptor (the fullerene molecules), with

crystalline domains on the nanometer length scale, and a composition gradient normal to the device electrodes. The optimum size of the nanodomains represent a compromise between good charge transport (large interconnected domains that form percolating pathways) and efficient charge generation (i.e. large exciton dissociation rate, which requires domains around twice as big as the exciton diffusion length, ~ 10´s nm) [8, 9]. The composition gradient improves the contact selectivity thus reducing the leakage current.

Moreover, the post-deposition treatments, and in particular thermal annealing, have also an additional positive effect: they -in principle- increase the OPV stability by means of the concomitant stabilization of the active layer blend compared to the frozen non-equilibrium morphology of the as cast films [9]. This is particular important if one takes into account that the relatively low glass transition temperatures that most soluble conjugated polymers exhibit may cause a morphology change as the temperature significantly rises during device operation [9]. In the process of stabilizing the morphology, thermal annealing does, however, also yield large scale phase separation [8, 10-12]. For instance, annealing at 140$^{o}$C for one hour a 1:1 (in weight %) regio regular P3HT:PCBM blend film leads to micron size PCBM clusters (see Figure 1(a)) which are not beneficial to OPV performance. The fabrication of OPVs with appropriate control over the nanostructure is, therefore, a key challenge for which currently only a few general rules –regarding optimum composition- have been found [11].

In this paper we investigate the possibility of using ternary mixing in order to control the blend morphology. The rationale is that small amounts of an amorphous polymer may form a dilute matrix which would allow the formation of small crystallites but prevent the large scale phase separation of the components. For devices based on blending PCBM with P3HT of two different molecular weights [13], it was observed that the advantages of both low molecular weight (efficient charge generation) and high molecular weight (enhanced transport) could be combined and thus this type of *ternary* mixing resulted in enhanced

device performance. Here we have chosen ternary blends of PCBM with regio regular (RR-) P3HT and regio random (RRa-) P3HT. We will show that besides a very efficient control of the blend morphology, regio random P3HT also adds several other functionalities, such as energy transfer to the more crystalline RR-P3HT, enhanced charge generation and improved open circuit voltage, all with minimum cost in terms of charge carrier mobility. The final ternary based devices, even without optimization procedure, are some 20% more efficient than the conventional annealed blends when excited with low intensity monochromatic light.

## 2 Experimental section

### 2.1 Materials and thin film fabrication

Regio regular ((Aldrich #669067, regioregularity >95% head-to-tail regioregular (HNMR), Mn = 17500) and regio random poly(3-hexylthiophene) P3HT ((Aldrich #510823, regioregularity=1:1 (head-to-head):(head-to-tail) linkages of regioisomers, no data available of Mn) were purchased from Aldrich and used as received. Herein, regio regular and regio random materials will be denoted RR-P3HT and RRa-P3HT, respectively. [6,6]-phenyl $C_{61}$-butyric acid methyl ester (PCBM) was obtained from Luminescence Technology and also used as received.

Binary blends consisting of RR-P3HT and RRa-P3HT were prepared from different solution concentrations (from 15g/l, to 50g/l) in high grade chlorobenzene, and spin coated at varying spin speeds (2000 to 4000 rpm) so to produce different thicknesses. The relative concentration of regular and random (RR-P3HT:RRa-P3HT) polymers were varied in 0.25 steps: (1:0), (0.75:0.25), (0.5:0.5), (0.25:0.75) and (0:1). The mobility on binary systems was measured in devices containing around 150 nm thick films deposited from a total 50 mg/ml solution.

For ternary blends, total 60mg/ml solutions in chlorobenzene were prepared, from which 30mg were PCBM, and the other 30mg split between RR-P3HT and RRa-P3HT, so to finally produce constant (1:1) fullerene:(polymer) concentrations. The relative content of regular and random was varied leading to the following PCBM:RR-P3HT:RRa-P3HT concentrations (1:1:0), (1:0.9:0.1), (1:0.75:0.25), (1:0.5:0.5), (1:0.25:0.75) and (1:0:1). Herein, we denote *conventional blend* the films comprising the (1:1:0) ratio, i.e. (1:1) PCBM:RR-P3HT, and it will be used as reference. Moreover, a different set of devices was fabricated from solutions made by adding RRa-P3HT to a 1:1 PCBM:RR-P3HT (60mg/ml) solutions, ending up in the following relative concentrations: (1:1:0.1) and (1:1:0.25). For the devices, a two step process was identified during spin speed optimization: 1000 rpm for 3 s in order to produce a homogeneous distribution of the solution throughout the substrate, followed by 90 s at 2000 rpm. This protocol typically resulted in active layers with thickness in the 85-105 nm range.

The solutions were spin coated on cleaned quartz substrates or ITO covered glass (150 nm thick ITO layer with a sheet resistance of 10 Ω/sq, SLR grade, Sanyo Vacuum Industries Co. Ltd). For the solar cells, PEDOT:PSS (Baytron P VP Al 4083 (H.C. Starck)) was spin coated (3000 rpm for 90 s) onto the ITO coated glass and annealed at 200$^{o}$C for 20 min. The ternary systems were thermally annealed at 140$^{o}$C for 1h inside a nitrogen-filled Glovebox ($O_2$ and $H_2O$ levels less than 2 ppm).

### 2.2 Thin film characterization

Film thicknesses were measured using a Dektak 3030 profilometer (and double checked with the thicknesses deduced from the absorption data using the optical constants from Ref. [8]). Scanning laser microscopy images were taken using a Keyence VK-9700 microscope. At least 10 images were employed for each sample in order to obtain average values of the density of large scale (micron size) aggregates of PCBM. Atomic Force Microscopy (AFM) was carried out with

a SPA 400 system by Seiko Instruments, Inc. Typically, at least three AFM images were taken for each sample and their surface roughness was analyzed using the Spisel 32 piece of software. X-ray diffraction (XRD) experiments were conducted using a Material Analysis and Characterization SRA system, model M18XHF, which employs a CuK$\alpha$2 source (40KV, 60mA) with wavelength 0.1544390 nm. Upon background removal, the data were fitted with a Gaussian function in order to obtain the peak intensity, width and angular position at the maximum. These data were then used to deduce the average interplane distance within the crystallites (from Bragg's law), estimate crystallite size (from Scherrer's relationship), and overall degree of crystallinity (integrating the area underneath the XRD peak).

The thin film absorption spectra were measured using a Perkin Elmer Lambda750 UV/Vis spectrometer from 300 nm to 800 nm. Photoluminescence (PL) data were collected using a Perkin Elmer LS55 Fluorescence Spectrometer. Unless otherwise stated, the PL excitation wavelength was set to 450 nm (around the absorption maximum for RRa-P3HT).

Pristine polymer films deposited onto pre-cleaned ITO/glass substrates were used to measure the HOMO levels of the polymers by means of a Riken Keiki AC-2 ultraviolet photoelectron spectrometer. The experimental set up is similar to that of conventional UPS but it does not require vacuum. On the other hand, the precision of our apparatus is smaller than that of a conventional UPS in vacuum, with uncertainty values ~ 0.03 eV. Using ultraviolet photoelectron spectroscopy we obtained a HOMO value of 4.61 ± 0.03 eV for regio regular P3HT, whilst that of regio random P3HT was found to be 4.73 ± 0.03 eV. The slightly smaller values obtained here for RR-P3HT (often around 5 eV) might be related to possible effects of the ITO surface on the measurement. We note that two samples with different thicknesses were measured for each polymer, and each sample was measured twice. The deviation between measurements and samples are smaller than the 0.03 eV uncertainty values.

## 2.3 Device fabrication and characterization

Single carrier devices were fabricated and the dark current-voltage characteristics measured and analyzed in the space charge limited (SCL) regime following the references [4] and [14]. Hole only devices consisted on the active material (binary or ternary system) spin coated onto Glass/ITO substrates, and capped with a 5 nm evaporated $MoO_3$ layer followed by a 100 nm thick Al contact. The evaporation mask defined 4 pixels in each sample with a 4 $mm^2$ area for each pixel. For the electron only devices, the structure was Glass/ITO/Al/blend/Ba/Al, where both, Ba and Al were evaporated. High-purity $MoO_3$ (6N grade, Mitsuwa Chemicals Co., Ltd), Ba (Aldrich), and Al (AL-011480, Nilaco Co.) source materials were employed as delivered. The standard deviation of the fit to the SCL equations for the electron only devices was slightly higher than that for the hole only devices, indicating a larger error on the extracted electron mobilities. The reported mobility data are average values over the four pixels of each sample at a given film composition.

For the solar cells, the active blend was spin coated on top of PEDOT:PSS coated Glass/ITO substrates in a clean room, and then transferred into an interconnected Glovebox where the Al electrode was thermally evaporated. Thermal annealing of the devices was done inside the Glovebox before the deposition of the contacts. All of the devices were encapsulated with a glass cap using an ultraviolet curing epoxy resin. The 15 min exposure to the UV radiation was performed from the Al metal side to avoid photodegradation of the organic layers across the active region.

The current-voltage characteristics of the encapsulated devices were measured outside the Glovebox, using a semiconductor characterization system (SCS4200, Keithley Instruments Inc.) at room temperature. For light J-V and EQE measurements, the above instrument was coupled to a JASCO CT-25C grating monochromator which selects the wavelength coming from a USHIO Optical

Modulex light source. The intensity of the monochromatic light was fixed at 20μW after calibration against a standard Coherent Fieldmaster photodiode with circular detecting area of 8mm in diameter (resulting in a illumination density of 400 mW/m$^2$). In order to explore the light intensity dependence of the solar cell parameters, the light intensity was varied using optical density filters between 0.3 μW and 45 μW. The encapsulated devices were kept in air and darkness for 10 months, when some of them were measured again to check the variation in performance with time.

## 3 Results and discussion

### 3.1. Characterization of binary and ternary systems

Figure 1 (a) shows a representative laser microscopy image of a conventional PCBM:RR-P3HT (1:1) blend film annealed at 140$^o$C for 1h. To start with, annealing leads to the appearance of large size aggregates as clearly seen in the image. These aggregates, which are not present in the as spun films, are rich in PCBM molecules [8, 11] and are surrounded by a polymer rich region, seen here as a halo like structure. It has been shown that PCBM nucleates into these aggregates upon annealing [8], or, in other words, once they are large enough to be seen using a microscope, they grow bigger in size, but their number remains constant. The average diameter of the region containing one PCBM aggregate and the associated P3HT halo is around 13 microns (see Fig. 1(b)), in good agreement with previous reports [8].

[Figure 1]

Such a large phase separation is, in principle, detrimental for solar cell performance since it is several orders of magnitude larger than the exciton diffusion length (~ tenths of nm's), and thus charge generation is strongly inhibited on those regions. By averaging over ten microscope images across the sample, we estimate the density of PCBM micron size domains to be around 700 aggregates per square mm. If we consider the average size of the aggregates,

this means that around 9% of the area is covered with these structures, and thus, 9% of the film is not acting positively as light-to-electricity converter. The introduction of the regio random polymer into the blend has a marked effect on the structure of the film. Substituting the 25% of the RR-P3HT by RRa-P3HT (1:0.75:0.25 sample, Fig. 1 (c)) already decreases in more than two orders of magnitude the density of these large aggregates, down to just 3 aggregates/$mm^2$. This represents less than 0.04% of the total film area. The density is further reduced for larger amounts of the RRa-P3HT polymer in the ternary system. The samples with compositions 1:0.5:0.5 and 1:0.25:0.75 have 1 aggregate/$mm^2$ and 0.15 aggregates/$mm^2$, respectively (not shown). It is clear that this approach is extremely efficient at controlling the microscopic morphology of the blend films.

An important question that needs to be answered is whether the introduction of the RRa-P3HT chains yields an overall amorphous structure, not only at the micron level, but also down to the nanoscale. If the resulting morphology was totally amorphous, the mobility would likely fall and the absorption would be blue shifted, and as a consequence, the overall solar cell performance would be poor. As we will see below, the RR-P3HT chains can still crystallize in the ternary blends and, in addition, the extent of the phase separation is now greatly controlled with microscopic scale phase separation being almost totally suppressed. We will come back to this point below. The eventual appearance of micron sized aggregates also in ternary systems containing RRa-P3HT (<3 aggregates/$mm^2$) is, in most cases, associated with film defects, such as edges of the substrate, in which inhomogeneities in film composition might be present. An optimization of the film fabrication conditions may, therefore, lead to an even smaller number of large size aggregates in films based on ternary blends.

The advantages of controlling the large scale phase separation by using RRa-P3HT rather than other amorphous conventional polymers, such as polystyrene or polymethylmetacrylate, is two fold. First, we expect high chemical affinity amongst the blended materials due to the common backbone between RRa- and

RR-P3HT polymers. Other glassy polymers could promote an even larger phase separation if the interaction between chains overcomes the entropy increase granted by mixing (following Flory's theory of mixing). Optical and atomic force microscopy images show no evidence of large scale phase separation in RR-P3HT:RRa-P3HT binaries or in ternary blends (see details below). Second, a perhaps even more importantly, RRa-P3HT can act as an active matrix, helping the proper functioning of the devices and even adding functionality. In the following, we demonstrate several examples of this added functionality of the multicomponent system.

[Figure 2]

Figure 2 shows the normalized absorption (solid lines) and photoluminescence emission (dashed lines) of RRa-P3HT (blue) and RR-P3HT (red). The red shift spectra of the regular polymer compared to the random is associated to different molecular packing morphologies. Regio regularity enables a better ordering of chains into lamella crystallites where the polymer adopts a planar conformation with longer conjugation lengths and fewer defects, such as twists and radicals on the chains [15, 16]. Regio random chains form, on the other hand, glassy films whose optoelectronic properties are governed by individual chain processes [15, 16]. The crystallization of P3HT results in the appearance of pronounced structures in the absorption and PL spectra –phonon replica- not present in the data for RRa-P3HT films. Interestingly, the long wavelength shoulder observed in the absorption of RR-P3HT has been assigned to 2 dimensional excitations [17, 18], and hence is a direct consequence of the good interchain interactions within the crystallites. The intensity of this shoulder has, in fact, been found to be directly proportional to the X-ray deduced overall degree of P3HT crystallinity in P3HT:PCBM blend films subjected to various annealing treatments [19]. Another indication of the degree of chain interaction is given by the PL quantum efficiency, $\eta$. Jiang *et al* showed that RRa-P3HT has a much larger $\eta$ (~8%) compared to RR-P3HT (~0.5%) [15] due to the isolation of chains in the random case. Here,

we also found that RRa- films exhibit more than one order of magnitude higher PL than RR-P3HT films with comparable thicknesses (see Fig.3 (b)). It is thus apparent that regio-regularity strongly determines the degree of interchain interaction [16].

From the electronic point of view, one important effect of the aforementioned interactions is that the band gap of RR-P3HT is some 0.3eV smaller than that of RRa-P3HT, as estimated by extrapolating the absorption edge. This implies that RR-P3HT will be more appropriate for harvesting light in the red and infrared parts of the sun spectrum. Charge mobility will also depend on the interaction between neighboring chains [17] and, in fact, hole mobility in RRa- is several orders of magnitude lower than for RR-P3HT (we will come back to this point below). Therefore, in order to ensure good charge generation (and short circuit current) in OPVs based on ternary systems, the amount of RRa-P3HT should, in principle, be *small* compared to that of RR-P3HT.

Enhancing the interchain interactions typically leads to the splitting of the HOMO and LUMO levels (e.g. by means of Davydov splitting). Quantum chemical calculations have shown that bringing polymer chains closer together decreases (in absolute terms) the HOMO level [20]. The glassy morphology of the RRa-P3HT films can be associated to an effective isolation of the polymer chains, and thus, one may expect a larger (again in absolute terms) HOMO level [15, 20]. Using air ultraviolet photoelectron spectroscopy we found a 0.12 eV shift comparing the two polymers, with higher HOMO for RRa-P3HT, as expected from the argument above. On the other hand, the open circuit voltage ($V_{oc}$) in OPVs is proportional to the difference between the HOMO of the electron donor (polymer) and the LUMO of the electron acceptor (fullerene) [21], and thus one may expect an enhancement in the $V_{oc}$ values for OPVs based on ternary systems. This is, in fact, what is experimentally observed, as we will show.

[Figure 3]

Figures 3 (a) and (b) show the absorption and emission spectra, respectively, of binaries consisting of a varying concentration of RR-P3HT:RRa-P3HT, as well as the pristine materials for reference. The spin coating conditions were controlled in order to have films with comparable thicknesses (~ 80 nm). The dotted lines in Figure 3 (a) correspond to a linear addition of the absorption of the pristine materials weighted by the composition fraction of each material. For instance, the absorption of the 0.75:0.25 binary is simulated (with no fitting parameters) by adding the absorption of RR-P3HT multiplied by 0.75 and the absorption of RRa-P3HT multiplied by 0.25. The surprisingly good agreement between the measured and simulated data suggests that, on the one hand, there is not strong interaction between the two polymers in terms of absorption (no new steady state species are created), and on the other side, the crystallization of RR-P3HT is not inhibited by the presence of the random chains. The latter is very important, especially after Chirvase and co-workers pointed out that PCBM molecules prevent the crystallization of RR-P3HT, which is only restored upon thermal annealing [10]. We note that the data shown in Figure 3 correspond to non annealed binary films.

The PL spectra for binaries cannot, however, be modeled using a linear combination of the PL spectra of the pristine materials. The addition of a small amount of RR-P3HT (25%) reduces the PL yield by six fold, almost down to the level of RR-P3HT (see Fig. 3(b)). Given the good spectral overlap between the emission of RRa-P3HT films and the absorption of RR-P3HT (see Fig. 2), energy transfer from the random to the regular chains seems a plausible explanation for this. Comparison between the PL recorded using two different excitation wavelengths (450 nm and 550 nm, the latter being the maximum absorption for RR-P3HT, not shown) also points towards this explanation. Whether is a real (re-absorption) or a virtual (energy transfer properly speaking) process of transferring the absorbed photon energy from regio random to regio regular, or even a combination of both, is not clear at this stage. In any case, the PL spectra

strongly indicates that the transfer is actually happening and thus the absorption of light in the regio random chains is followed by a transfer of a substantial part of that energy to regio regular material where electrons are excited and through which the transport of carriers can be greatly facilitated. A detailed time-resolved study on the PL dynamics could bring useful information in this respect.

The efficient charge transfer (exciton dissociation) between the polymer chains and fullerene molecules, necessary step for charge generation, is often seen experimentally as a strong reduction in the PL quantum yield upon blending the polymer with the fullerene molecules. PCBM is an extremely efficient PL quencher in both cases RR- and RRa-P3HT (contrast for instance Fig. 3(b) and 4(b)). Comparing the PL exhibited by films containing the same amount of polymer with and without PCBM, it is possible to estimate the degree of PL quenching. It turns out that the PL quenching is much more pronounced (~50 times more) in RRa-P3HT than in RR-P3HT. The most likely reason for this is the finer intermixing between components achieved in PCBM:RRa-P3HT films compared to the conventional blend, resulting from the glassy morphology of the random polymer with very little –or even none- tendency to crystallize. It has been shown that the crystallization of P3HT is, in fact, one of the main factors driving the diffusion of PCBM molecules into phase separated regions [8] and thus, a non-crystallizing polymer (such as RRa-P3HT) may accommodate more easily the fullerene molecules within polymer chain voids. This view is supported by the lack of micron-sized PCBM aggregates in the ternary systems: fullerene molecules are somehow anchored in the voids left by the dilute random matrix. AFM images of PCBM:RRa-P3HT films show no evidence of phase separation and the corresponding surface roughness remains extremely small (<0.6 nm) after mixing the random polymer with the fullerene molecules. Therefore, random P3HT might, interestingly, lead to an efficient charge generation due to the resulting morphologies of their films. Ternary systems show a gradual decrease in the PL intensity with increasing RRa-P3HT concentration, as shown in Figure

4 (b), which suggests an increased capability for PL quenching, or exciton splitting with adding RRa-P3HT.

[Figure 4]

As for the case of the conventional PCBM:RR-P3HT blends, the incorporation of the fullerene molecules precludes the formation of P3HT crystallites in the as spun films also in the ternary systems. Similarly, thermal annealing (at 140$^{o}$C for 1 hour) enhances the crystallization also in the ternaries. Figure 4 (a) shows the absorption spectra for annealed ternary blends. Judging by the ratio of the intensities of the maximum and the shoulder centered at around 650 nm, one may risk to say that ternary blends are equally, or even slightly more, crystalline (in relative terms) than the conventional binary [22].

[Figure 5]

Surface roughness, as obtain from AFM images, have often revealed the degree of crystallinity in the films underneath (see e.g. Ref [23]). We have taken AFM images of the ternary systems and confirm the increase in roughness (crystallinity) upon annealing suggested by the absorption spectra. Figure 5 (a) and (b) compare the morphology of a film based on the conventional blend before and after thermal annealing, respectively. The Ra surface roughness increases from 0.6 to 0.7 nm upon annealing. All of the as-spun ternary films are smoother than the conventional blend, but, interestingly, the surface roughness for the ternaries increase to larger values than that of the PCBM:RR-P3HT blend with annealing (see e.g. Figures 4(c) and 4(d) and Table I). This may again suggest that the degree of crystallization is larger in ternary systems than in the conventional blend. However, another possible explanation could be that the three components are phase separating and thus producing a rougher surface. For comparison, it might be noted that the Ra roughness of the pristine RR- and

RRa-P3HT films is 6.6 nm and 0.3 nm, respectively. The AFM deduced roughness values for the ternary films are summarized in Table I.

[Table I]

In order to get a better understanding of the aforementioned phenomena suggested by the absorption and AFM data, we have performed X-ray diffraction (XRD) measurements on annealed ternary films. The data for these experiments is shown in Figure 5(e), including that of the pristine RR-P3HT film used here as reference. The material parameters deduced from the analysis of the results are summarized in Table I. We note that the sample containing only regio random P3HT does not show any diffraction peak, in accordance to the expected lack of crystallinity. Our deduced 1.72 nm interplane distance (following Bragg's law) agrees well with previous data for P3HT [19]. Moreover, it seems to slightly increase from 1.72 nm to 1.76 nm with increasing RRa-P3HT concentration from 0% to 75% in the total polymer content. Although we do not have a full explanation for this, it might be due to the fact that the regio regular crystallites are immerged in a soft matrix of the random material, which may shrink in order to accommodate the expanding (through annealing) regio regular crystallites; while in the case of the conventional blend, the crystallites cannot expand because they might be in contact with other, equally hard, crystallites. If this was the case, it might be interesting to see the effect that a semicrystallizing matrix that formed harder crystallites would have on the interplane distance (and even hole mobility) of P3HT:PCBM blends. Some support for this very initial hypothesis may come from the fact that when the effect of a rigid substrate interface is made apparent (by decreasing film thickness), P3HT chains pack into different type of crystallites [24].

The RR-P3HT crystallite size was estimated using Scherrer's relationship and the average sizes we find are larger than those reported by Zhokhavets et al [19], as one could expect given the fact that our annealing times are much longer (1h

in our case, and 5 mins in theirs). Importantly, as the content of regio random is increased, the crystallite size is greatly reduced from around 16 nm for the PCBM:RR-P3HT:RRaP3HT (1:1:0) film to ca 10 nm for the (1:0.25:0.75) sample. This suggests that there might be an increase in polymer chain entanglement with increasing random concentration which prevents the formation of large crystallites. We note that we have employed only the optimum annealing temperature for the conventional blend, and thus there is room for optimizing the thermal annealing procedure for the ternary systems which may require longer annealing times, or higher annealing temperatures to create crystallites of the same size as the conventional blend.

By integrating the area of the XRD peak, one may obtain a measure of the degree of crystallinity of the film [19]. Interestingly, this evaluation again indicates that ternary systems are more crystalline than the conventional blend (see Table I), in agreement with the absorption and AFM data, and thus rules out the hypothesis of the large scale phase separation of the three materials as the main explanation of the increased roughness in annealed ternary films compared to the conventional binary.

Therefore, all of the evidences suggest that the structure of ternary films consists of crystallites of regular P3HT -of smaller size than those found in the conventional blend- embedded into a random polymer matrix, and where PCBM can only form small aggregates and not the micron size structures often observed in the conventional case. Figure 1(d) and 1(f) schematically depict the nanomorphology of the conventional binary and the proposed ternary systems, respectively. The study of the ternary system phase diagram would also be interesting to gain further insight into the phase separation capabilities of the materials as well as optimum temperatures and compositions [11].

Summarizing the main results up to now, from a structural point of view, the random P3HT chains define a dilute matrix, or soft scaffolding, within which

crystallites of the regular P3HT chains and aggregates of PCBM molecules can be formed in a controlled fashion (using the available but limited free volume), preventing large scale phase separation of the components.

### 3.2 Charge carrier mobilities

In order to understand the effect of ternary mixing in the carrier mobilities, devices have been fabricated in which the active blend film was sandwiched between two contacts that were selected in a way so to obtain hole only or electron only devices (see Experimental section). By varying the film thickness we identified the range of thicknesses in which the current voltage characteristics are governed by the space charge limited (SCL) regime. We then deduced the zero field hole and electron mobilities by fitting the current-voltage curves following Refs. [4] and [14]. Figure 6 (a) shows three representative cases. The experimental points (symbols) are very well fitted with the SCL equation for over 3 to 4 orders of magnitude in the values of the current density.

[Figure 6]

Figure 6 (b) shows the SCL deduced hole (circles) and electron (squares) mobilities for binary (solid symbols) and annealed ternary (open symbols) systems. Each data point is the average of the mobility values extracted from four devices. The hole mobility values obtained for the conventional blends agree well with those reported in the literature for annealed samples [4] (~$1.2 \cdot 10^{-8} m^2 V^{-1} s^{-1}$). As for the electron mobility, our values are slightly smaller than those reported, perhaps due to a possible small partial oxidation of the evaporated Al electrode before the spin coating of the active blend, or to a small underestimation of the electron mobility values resulting from higher fitting standard deviations. Regio random P3HT shows a hole mobility of almost five orders of magnitude lower than that of regio regular. Interestingly, this value (~$5 \cdot 10^{-13} m^2 V^{-1} s^{-1}$) is not very far from the hole mobility values of ~$3 \cdot 10^{-12} m^2 V^{-1} s^{-1}$ exhibited by non-annealed (or low temperature annealed) regular P3HT blended

with PCBM [4]. It seems clear, therefore, that the low mobility of RRa-P3HT is the result of lack of crystallinity and the associated weak interchain interactions (c.f. RR-P3HT).

Perhaps the most important result in this section is the finding that the carrier mobilities are only slightly affected by the introduction of this -very low mobility- polymer. Amazingly, substituting the 75% of the regio regular chains by regio random chains in the ternary system only decrease the hole mobility from ~1.2•$10^{-8}$$m^2V^{-1}s^{-1}$ to ~3.5•$10^{-9}$$m^2V^{-1}s^{-1}$, i.e. less than one order of magnitude. For comparison, it is worth noting that thermally annealing has a much stronger effect on charge transport: the as spun conventional blend has almost four orders of magnitude lower hole mobility compared to the thermally annealed (at 130 $^{o}$C-150 $^{o}$C) case [4]. However, this interesting result may not be unexpected on the light of the morphology investigations reported above: absorption, photoluminescence, AFM and XRD data all indicate that the ternary systems are also highly crystalline. Goffri et al have also found a similar behavior for the field effect transistor hole mobility of P3HT blended with semicrystalline commodity polymers [25], so perhaps this is a relatively general trait of semiconducting polymers independent of whether mobility is measured across the film thickness or in the perpendicular direction, and even at totally different carrier density values. There are two possible readings for this phenomenon. First, the material percolation threshold requires very little amount of the crystallizing component (less than 25% in our case), probably due to the extended length of the polymeric macromolecule. A second interpretation could be, however, that most of the film is, in practice, not contributing (at least positively) to the transport of charges. The second possibility opens one important question: how could one process a film so to employ the 100% of the material to actively participate in the charge transport? This key question has, to our knowledge, not being answered yet.

The slight mobility decrease might be related to smaller crystallite sizes. We find a linear relationship between charge mobility and crystallite size, with the holes

having a stronger dependence (in terms of the slope of the fitted straight line). On the other hand, the mobility values do not seem to be so clearly related to the overall degree of P3HT crystallinity, i.e. when plotted together, the experimental points scatter through the graph with no distinguishable trend. This apparent contradiction was also observed in pristine P3HT films with different molecular weights: lower molecular weight P3HT is much more crystalline but, nonetheless, its mobility is lower compared to that of higher molecular weight P3HT [26, 27]. This can be explained in terms of poorer connectivity and more insulating grain boundaries for the more crystalline polymer [26]. This explanation could be perfectly applied here, since smaller crystallites (even at a constant total crystallinity) would exhibit many more grain boundaries than larger crystallites. It is important to emphasize that, compared to the almost four orders of magnitude changes in field effect mobility [26] (or 15 times in the SCL mobilities [27]) observed when increasing the number average molecular weight from 3.2 to ca 40 kDa, in our case the effect is very mild, with a decrease in zero field mobility of less than one order of magnitude when substituting the 75% of the RR-P3HT by RRa-P3HT.

It is important to note that binary and ternary systems have very similar hole mobilities for RRa-P3HT concentrations smaller than 50% with respect to the concentration of RR-P3HT. However, it seems that the percolation threshold for the binary happens at higher random concentration than in the ternary system. The thermal annealing (only applied here to the ternaries) may help to enhance hole mobility in the ternary systems containing 75% of regio random, when compared to the values for non-annealed binary RR-P3HT:RRa-P3HT blends with also 75% or RRa-P3HT, even when the crystallinity of the binaries is expected to be high according to their absorption spectra (Figure 3(a)). Alternatively, this difference between binary and ternary blends may support the report by Tuladhar and co-workers [28], which were able to demonstrate that PCBM not only helps to enhance the hole mobility of the polymer by a possible modification of the polymer chain packing, but they also found that the hole and

electron mobilities deduced using the Time of Flight technique for a system consisting of PCBM embedded into an insulating polystyrene matrix have a similar value, independently of the film thickness. This strongly indicates that PCBM actively contributes to the hole mobility (polystyrene is an insulator). In other words, comparison between the mobility values deduced for regular:random binaries and the ternary systems may indicate that PCBM is also actively enhancing the hole mobility in our case.

### 3.3. Solar cells based on ternary systems

Figure 7 shows the performance of solar cells based on ternary blend films with different RR- to RRa- composition ratios, and keeping the overall polymer to fullerene weight ratio constant (1:(X:Y)) with X+Y=1. The current density vs. voltage curves measured at monochromatic light (550 nm, 20$\mu$W) show two clear trends with increasing regio random composition in the ternary: i) decrease in the $J_{sc}$; and ii) increase in the $V_{oc}$. Table I summarizes these values.

[Figure 7]

The case of the $V_{oc}$ can be understood in terms of the increase in the relative importance of the regio random chains in the charge generation. As we discussed above, the non-interacting chains of RRa-P3HT yield a higher HOMO compared to the crystalline P3HT [15, 20]. Since the $V_{oc}$ is proportional to the difference between the energy levels of the donor HOMO and acceptor LUMO [21], an increase in the polymer HOMO may be responsible for the observed increase in $V_{oc}$. This conclusion is supported by a recent study made with polythiophenes with different alkyl chain lengths (P3AT). It was found that the $V_{oc}$ of annealed devices made with different P3ATs increases from 500 mV to 600 mV with increasing alky length -and thus reducing interchain interactions- from butyl to dodecyl [29]. A very recent report [30] on solar cells based on the addition of higher-HOMO level MDMO-PPV chains to the conventional

PCBM:P3HT blends, also shows improved $V_{oc}$, and thus again supports our hypothesis.

It is important to note that the increase in $V_{oc}$ is not linearly proportional to the amount of RRa-P3HT, but, instead, it has a strong effect already for low random concentrations and then saturates at about 50%. This can be understood in terms of the resulting ternary blend morphology, since the PCBM molecules might accommodate themselves more easily in the polymer voids left by the amorphous RRa-P3HT matrix than to be embedded into the RR-P3HT crystallites. This interpretation is supported by the PL quenching data showed in Figure 4(b). The measured superlinear behavior in the enhancement of $V_{oc}$ with increasing RRa-P3HT content relaxes the apparent compromise between the observed opposite trends of $J_{sc}$ and $V_{oc}$.

With respect to the decrease in the $J_{sc}$, it may be associated to the combination of two main factors: 1) a decrease in the absorption of the ternary active layer at 550 nm; and 2) a decrease in carrier mobility with increasing RRa- content. To evaluate the relative importance of these two factors, we have plotted in Figure 7 (b) the J-V characteristics normalized by the absorption of the films at 550 nm. From this graph, it seems that there are two distinct regimes: up to concentrations containing 50% of RRa-, the effect of reduced mobility is only small, however, for larger amounts of the regio random polymer the polymer percolation threshold for good device operation is overpass and then the $J_{sc}$ drastically falls.

We have recently demonstrated a similar compromise between $J_{sc}$ and $V_{oc}$ in organic solar cells using another approach but with a similar argument in terms of the energy levels of the active materials [31]. By inserting an ultrathin metal-phthalocyanine layer (CuPc or ZnPc, HOMO ~ 5.1 eV) at the bilayer interface between pentacene (HOMO ~ 5.0 eV) and fullerene, a higher $V_{oc}$ was observed. The $V_{oc}$ increased with increasing CuPc or ZnPc layer thickness as a result of the

higher HOMO level, however, the $J_{sc}$ decreased due to the lower mobility of the phthalocyanine compared to that of pentacene [31]. A compromise in phthalocyanine thickness was found between enhanced $V_{oc}$ and reduced $J_{sc}$ so to finally obtain higher device efficiencies. Similarly, in the ternary blends case, increasing in excess the concentration of the low mobility random chains can lead to surpassing the threshold composition for percolation of the highly conductive regio regular P3HT chains and thus the photocurrent drops. However, the compromise between device parameters in the ternary blends is much more relaxed, as we will show below.

It is worth noticing that there could be an alternative explanation for the observed trends in photocurrent and open circuit voltage. This interpretation is based on the idea that the addition of the random chains may result in a different recombination constant. Assuming that the theory of Langevin recombination is valid in the ternary systems, a reduction of the mobility could cause a reduction of the recombination constant and therefore a lower photocurrent and a higher open circuit voltage, as it is sometimes observed in OPV systems based on polymers with low charge carrier mobilities [32]. As we will see, the fact that we can decouple the effect in $J_{sc}$ and $V_{oc}$ for low RRa-P3HT concentrations may suggest that this effect is significant only for large RRa-P3HT relative concentrations.

The different absorption spectra for varying compositions (Fig. 3 (a)) are also reflected in the External Quantum Efficiency (EQE), as shown in Figure 7 (c). It is even possible to distinguish the RRa-P3HT absorption peak centered at around 450 nm in the EQE of the devices based on the 1:0.25:0.75 composition (top curve in bottom panel). This further indicates the active role that the random P3HT is playing in the solar cell. We note that the relatively large inhomogeneity of the light intensity through the beam spot lead to EQE uncertainties of the order of 5% in the deduced EQE values reported here.

[Figure 8]

Our results suggest that if the lower absorption is compensated for, small concentrations of RRa-P3HT could lead to overall better device performance by increasing $V_{oc}$ while keeping $J_{sc}$ constant. A straight forward way of doing this without the need for systematic optimization is to fabricate solar cells based on blends which keep constant the PCBM:RR-P3HT ratio (1:1), and then adding small amounts of the RRa-P3HT into the solution. Figure 8 shows the J-V characteristics under the same illumination conditions as above for devices based on ternary films with PCBM:RR-P3HT:RRa-P3HT compositions 1:1:0.1 and 1:1:0.25, as well as the 1:1:0 conventional blend for reference. As we have predicted, once the absorption of light at 550 nm is kept constant, the $J_{sc}$ shows an almost constant value within the experimental uncertainty. In fact, the EQE spectra at 0V for these three devices are almost identical (not shown). On the other hand, the $V_{oc}$ for solar cells based on ternary systems is clearly enhanced by more than 100 mV with respect to the reference conventional blend, as shown in Figure 8. This is fully consistent with the 0.12 eV increase in HOMO level for RRa-P3HT compared to RR-P3HT, as deduced here using ultraviolet photoelectron spectroscopy. Moreover, the fill factor also slightly improves by ternary mixing. Overall, there is a 20% increase in the maximum power obtained at 550 nm, $V_{max} \bullet J_{max}$ comparing the reference (1:1:0) and the sample with 25% added random polymer chains (1:1:0.25), which may indicate a 20% enhancement in efficiency in the current illumination conditions.

In order to check the evolution of device performance and morphology with time, these three samples (with four devices per sample) were measured again after a period of 10 months, through which they were kept on air and in darkness. These solar cells still work perfectly fine after this time span, which suggests that the glass encapsulation and darkness ambient conditions have prevented chemical oxidation of the active layers and interfaces. Nonetheless, there are some changes on the current/voltage curves after this time, which we, preliminary

assign to morphologic relaxation of the films over time. These changes over time are much larger than the pin to pin differences amongst the four pins in a given sample. The percentage change of the J-V curves (see Figure 9) when comparing the samples as fabricated and after 10 months is much more pronounced (~75% more) for the conventional binary than for the ternary based samples. These data suggest that the natural entanglement of the glassy amorphous RRa-P3HT chains helps to stabilize the film morphology and thus, positively contributes to increase the effective lifetime of the cells. These preliminary results are currently being systematically investigated in order to further test the hypothesis of improved morphological stability.

Figure 9

The OPV performance under varying light intensities shows that the $V_{oc}$ of the conventional binary based cells increases with light intensity towards the $V_{oc}$ of the ternary system cells (see Figure 9). This may suggest that the regular chains that do not form part of the crystallites, and thus are found in a more amorphous state, begin to participate on the photovoltaic action for higher light intensities, perhaps after the expected charge traps are filled. Our proposed ternary system based devices exhibit a less strong intensity dependence of performance (and always higher $V_{oc}$ regardless of the light intensity), as deduced from the slopes of the linear fits in Figure 9. This may be originated, as we have mentioned, by a reduced recombination constant arising from slightly lower mobilities in the ternary systems compared to the conventional blend [32]. This weaker dependence in light intensity could mean a significant advantage when this type of device is used in low light intensity applications such as highly sensitive photodiodes and solar cells placed indoors or at particular outdoor conditions (e.g. cloudy days or early and late hours of the day).

Figure 10

Although there clearly are a large number of parameters that could be further optimized, such as polymer molecular weights [26, 27], ternary composition [11, 25], thermal annealing treatment [4, 33] or film thickness [34, 35], it is patent that the presented strategy results in a more controlled blend structure and enhanced solar cell performance. The device optimization might be facilitated by the measurement of the phase diagram of the ternary system, which will aid to predict the optimum composition ratio and thermal annealing treatment [11]. Moreover, the natural entanglement of the glassy chains may also help to provide long term morphological stability, as suggested by our preliminary results, which would help to keep a constant performance of the devices under operation at elevated temperatures. Some of these investigations are currently being carried out and will be published elsewhere.

Finally, we believe that the ternary mixing approach is very general, and could be used to control the morphology at the micro- and nano- scales for a large variety of semicrystalline polymers with poor capability for quality film formation when blended with fullerenes and otherwise good optoelectronic properties. Examples of this include polythiophenes with different alkyl side chains, such as poly(3-butylthiophene) (P3BT) [29, 36], Selene substituted regio regular poly(3-hexyl)selenophene (P3HS) [37], or very low band gap regular poly(3-decyloxythiophene-2,5-diyl) (P3DOT) [38], to name but a few. Furthermore, other dilute polymer matrices might be used to add different functionalities, such as simultaneous optimization of charge generation and transport [13, 30] or chemical and mechanical stability [25], which could permit an overall more efficient and stable organic solar cell and thus bring closer the market uptake turn point of this technology.

**4 Conclusions**

To summarize, in this contribution we have investigated ternary systems consisting on adding regio random P3HT into the conventional regular P3HT:PCBM blends. The rationale for this was to be able control the formation of

microscale phase separation through the natural entanglement of random polymer chains, while allowing the formation of crystallites at the nanoscale in the voids left by the diluted polymer matrix. We successfully demonstrate that ternary mixing helps to control the morphology by reducing the area covered with unwanted micron size aggregates from 9% in the conventional blend, down to less than 0.04% for the ternaries. Moreover, the addition of random polymer chains does not prevent the crystallization of their regular counterparts and we found, in fact, that the overall degree of film crystallization is enhanced in the ternary blends, at the expenses of smaller crystallite sizes. This results in the fact that concentrations of up to 50% of the random polymer in the total polymer content have a very small effect on charge carrier mobilities, compared, for instance to the effects due to thermal annealing or molecular weight. Finally, we fabricated solar cells based on ternary systems and show that they exhibit a similar short circuit current but a ca 100mV positively shifted open circuit voltage which results in enhanced device efficiency. The origin of this shift is associated to a higher polymer HOMO arising from the isolated –non-interacting- nature of the random chains.

**Acknowledgments**

M.C.Q. would like to thank the Japan Society for Promotion of Science for granting a postdoctoral fellowship under which most of this research was carried out and also acknowledges the Japan Advanced Institute of Science and Technology (JAIST) for their great hospitality. The authors are very grateful to Mr. T. Nakayama (of JAIST) for the photoelectron spectroscopy measurements.

**References**

1. C. J. Brabec and J. R. Durrant, MRS Bulletin, 33 (2008) 670.
2. J. Y. Kim, K. Lee, N. E. Coates, D. Moses, T.-Q. Nguyen, M. Dante, A. J. Heeger, Science, 317 (2007) 222.
3. M. A. Green, K. Emery, Y. Hishikawa and W. Warta, Prog. Photovolt: Res. Appl. 17 (2009) 85.

4. V. D. Mihailetchi, H. Xie, B. de Boer, L. J. A. Koster, and P.W. M. Blom Adv. Funct. Mater. 16 (2006) 699.
5. S. E. Shaheen, C. J. Brabec, N. S. Sariciftci, F. Padinger, T. Fromherz, and J. C. Hummelen, Appl. Phys. Lett. 78 (2001) 841.
6. W. Ma, C. Yang, X. Gong, K. Lee, and A. J. Heeger, Adv. Funct. Mater. 15 (2005) 1617.
7. G. Li, V. Shrotriya, J. Huang, Y. Yao, T. Moriarty, K. Emery, and Y. Yang, Nat. Mater. 4 (2005) 864.
8. M. Campoy-Quiles, T. Ferenczi, T. Agostinelli, P. G. Etchegoin, Y. Kim, T. D. Anthopoulos, P. N. Stavrinou, D. D. C. Bradley and J. Nelson, Nat. Mater. 7 (2008) 158.
9. X. Yang and J. Loos, Macromolecules, 40 (2007) 1353.
10. D. Chirvase, J. Parisi, J. C. Hummelen and V. Dyakonov, Nanotechnology, 15 (2004) 1317.
11. C. Müller, T. A. M. Ferenczi, M. Campoy-Quiles, J. M. Frost, D. D. C. Bradley, P. Smith, N. Stingelin-Stutzmann and J. Nelson, Adv. Mater. 20 (2008) 3510.
12. E. Klimov, W. Li, X. Yang, G. G. Hoffmann and J. Loos, Macromolecules, 39 (2006) 4493.
13. W. Ma, J. Y. Kim, K. Lee and Alan J. Heeger, Macromol. Rapid Commun. 28 (2007) 1776.
14. T. Matsushima, Y. Kinoshita, and H. Murata, Appl. Phys. Lett. 91 (2007) 253504.
15. X. M. Jiang, R. Österbacka, O. J. Korovyanko, C. P. An, B. Horovitz, R. A. J. Janssen and Z. V. Vardeny, Adv. Funct. Mater. 12(2002) 587.
16. Tian-An Chen, Xiaoming Wu, and Reuben D. Rieke, J. Am. Chem. Soc. 117 (1995) 233.
17. H. Sirringhaus, N. Tessler, R. H. Friend, Science, 280 (1998) 1741.
18. M. Campoy-Quiles, J. Nelson, D. D. C. Bradley and P. G. Etchegoin, Phys. Rev. B, 76 (2007) 235206.

19. U. Zhokhavets, T. Erb, G. Gobsch, M. Al-Ibrahim, O. Ambacher, Chem. Phys. Lett. 418 (2006) 347.
20. D. Beljonne, J. Cornil, H. Sirringhaus, P. J. Brown, M. Shkunov, R. H. Friend, and J.-L. Brédas, Adv. Funct. Mater. 11 (2001) 229.
21. M. C. Scharber, D. Mühlbacher, M. Koppe, P. Denk, C. Waldauf, A. J. Heeger, and C. J. Brabec, Adv. Mater. 18 (2006) 789.
22. This argument is based on the proportionality between the crystallinity of the film and the intensity of the 650 nm shoulder found by Zhokhavets et al in Ref. 19.
23. Y. Kim, S. Cook, S. M. Tuladhar, S. A. Choulis, J. Nelson, J. R. Durrant, D. D. C. Bradley, M. Giles, I. McCulloch, C.-S. Ha and M. Ree, Nat. Mater. 5 (2006) 197.
24. D. M. DeLongchamp, B. M. Vogel, Y. Jung, M. C. Gurau, C. A. Richter, A. Kirillov, J. Obrzut, D. A. Fischer, S. Sambasivan, L. J. Richter, and E. K. Lin, Chem. Mater. 17 (2005) 5610.
25. S. Goffri, C. Müller, N. Stingelin-Stutzmann, D. W. Breiby, C. P. Radano, J. W. Andreasen, R. Thompson, R. A. J. Janssen, M. M. Nielsen, P. Smith ad H. Sirringhaus, Nat. Mater. 5 (2006) 950.
26. R. J. Kline and M. D. Mcgehee, J. Macromol. Scien. C: Pol. Rev. 46 (2006) 27.
27. C. Goh, R. J. Kline, M. D. Mcgehee, et al. Appl. Phys. Lett. 86 (2005) 122110.
28. S. M. Tuladhar, D. Poplavskyy, S. A. Choulis, J. R. Durrant, D. D. C. Bradley and J. Nelson, Adv. Funct. Mater. 15 (2005) 1171.
29. L. H. Nguyen, H. Hoppe, T. Erb, S. Günes, G. Gobsch and N. S. Sariciftci, Adv. Funct. Mater. 17 (2007) 1071.
30. Y. Kim, M. Shin, H. Kim, Y. Ha and C.-S. Ha, J. Phys. D: Appl. Phys. 41 (2008) 225101.
31. Y. Kinoshita, T. Hasobe and H. Murata, Appl. Phys. Lett. 91 (2007) 083518.

32. L. J. A. Koster, V. D. Mihailetchi, R. Ramaker, and P. W. M. Blom, Appl. Phys. Lett. 86 (2005) 123509.
33. H. Kim, M. Shin and Y. Kim, J. Phys. Chem. C, 113 (2009) 1620.
34. G. Li, V. Shrotriya, Y. Yao, and Y. Yang, J. Appl. Phys. 98 (2005) 043704.
35. K. O. Sylvester-Hvid, T. Ziegler, M. K. Riede, N. Keegan, M. Niggemann, and A. Gombert, J. Appl. Phys. 102 (2007) 054502.
36. H. Xin, F. S. Kim, and S. A. Jenekhe, J. Am. Chem. Soc. 130 (2008) 5424.
37. A. M. Ballantyne, L. Chen, J. Nelson, D. D.C. Bradley, Y. Astuti, A. Maurano, C. G. Shuttle, J. R. Durrant, M. Heeney, W. Duffy, and I. McCulloch, Adv. Mater. 19 (2007) 4544.
38. C. Shi, Y. Yao, Y. Yang and Q. Pei, J. Am. Chem. Soc. 128 (2006) 8980.

**Figure captions**

Figure 1. (Colour online) Comparison of the microscale morphology of the conventional blend and the ternary systems. (a)-(c) UV Laser microscope images of annealed ternaries with PCBM:regularP3HT:randomP3HT concentrations of (a) 1:1:0; (b) 1:1:0 (zoom-in detail); and (c) 4:3:1; (d)-(f) schematics of (d) a conventional PCBM:Regular P3HT blend; (e) dilute random matrix; and (f) ternary system comprising a dilute random P3HT matrix filled with crystallites of PCBM and regular P3HT.

Figure 2. (Colour online) Optical properties of the pristine polymer. Normalised absorption (solid line) and emission (dashed line) for Regio Random P3HT (blue) and Regio Regular P3HT (red)

Figure 3. (Colour online) Optical properties of binary systems. (a) absorption and (b) emission of Regular:Random P3HT binary films.

Figure 4. (Colour online) Optical properties of ternary systems. (a) absorption and (b) emission of ternary films with constant solution concentration (60mg/ml), and constant PCBM:polymer concentration (1:1), with varying relative concentrations of Regular and Random P3HT.

Figure 5. (Colour online) Investigation on the crystallinity of ternary systems. 3x3micron AFM images for 1:(1:0) (a) Non annealed, (b) annealed; and for 4:(3:1) (c) non annealed and (d) annealed. (f) XRD intensity for ternary systems and reference pristine regular P3HT.

Figure 6. (Colour online) Study of the carrier mobility in binary and ternary systems. (a) Typical current density versus voltage curves for a conventional blend (open squares), a ternary blend with composition 1:0.5:0.5 (open triangles) and regio random P3HT (open diamonds). The solid lines are the fits to the SCL

equations; (b) Hole (circles) and electron (squares) mobilities deduced for single carrier devices based on Regular:Random binaries (solid symbols) and ternary (open symbols) systems.

Figure 7. (Colour online) Solar cell characteristics for devices based on the ternary systems. J-V curves (a), J-V curves normalised by the absorption at 550 nm (b) and EQE (c) for devices based on ternaries with constant solution concentration (60mg/ml), and constant PCBM:polymer concentration (1:1), with varying relative concentrations of Regular and Random P3HT.

Figure 8. (Colour online) Solar cell characteristics for devices based on the ternary systems with equivalent short circuit current. J-V curves for devices based on ternaries with constant PCBM:Regular P3HT concentration (1:1), with added Regio Random P3HT 1:1:0 (open squares), 1:1:0.1 (filled triangles) and 1:1:0.25 (open down triangles).

Figure 9. J-V curves in logarithmic scale for PCBM:Regular P3HT concentration (1:1:0), (open squares, left panel) and with added Regio Random P3HT 1:1:0.1 (filled triangles, right panel) as prepared (solid lines) and after 10 months (dashed lines).

Figure 10. (Colour online) Solar cell characteristics as a function of the incident light intensity. Light intensity dependence of the open circuit voltage (top panel) and short circuit current (bottom panel) for a conventional blend (squares) and a 1:1:0.25 ternary blend (circles).

Table I. Summary of morphologic, photophysical and device parameters for ternary systems.

| | 1:1:0 | 1:0.75:0.25 | 1:0.5:0.5 | 1:0.25:0.75 | 1:0:1 |
|---|---|---|---|---|---|
| Interplane distance [nm] | 1.72 | 1.73 | 1.75 | 1.76 | NA |
| Crystallite size [nm] | 16.2 | 13.7 | 10. 1 | 9.8 | 0 |
| Crystallinity [arb.units] | 657 | 755 | 774 | 728 | 0 |
| Absorption (550nm) | 0.418 | 0.346 | 0.275 | 0.198 | 0.123 |
| lambda max Abs [nm] | 546 | 548 | 512 | 479 | 473 |
| Ra roughness [nm] | 0.7 | 1 | 1.2 | 0.9 | 1 |
| RMS roughness [nm] | 0.9 | 1.3 | 2 | 1.3 | 0.6 |
| Hole mobility [$m^2$/Vs] | 2.20E-08 | 9.12E-09 | 2.76E-09 | 3.48E-09 | - |
| Electron mobility [$m^2$/Vs] | 2.38E-09 | 8.41E-10 | 3.35E-10 | 1.77E-10 | - |
| $J_{sc}$[mA/$cm^2$] (550 nm) | 0.0119 | 0.0090 | 0.0064 | 0.0020 | 0.0001 |
| $J_{sc}$/Abs(550nm) | 0.0285 | 0.0259 | 0.0233 | 0.0102 | 0.0007 |
| 100*$J_{ma}$*$V_{max}$/Abs (550nm) | 0.534 | 0.577 | 0.518 | 0.204 | 0.003 |
| $V_{oc}$ [mV] (550 nm) | 331 | 384 | 390 | 391 | 147 |

Figure1

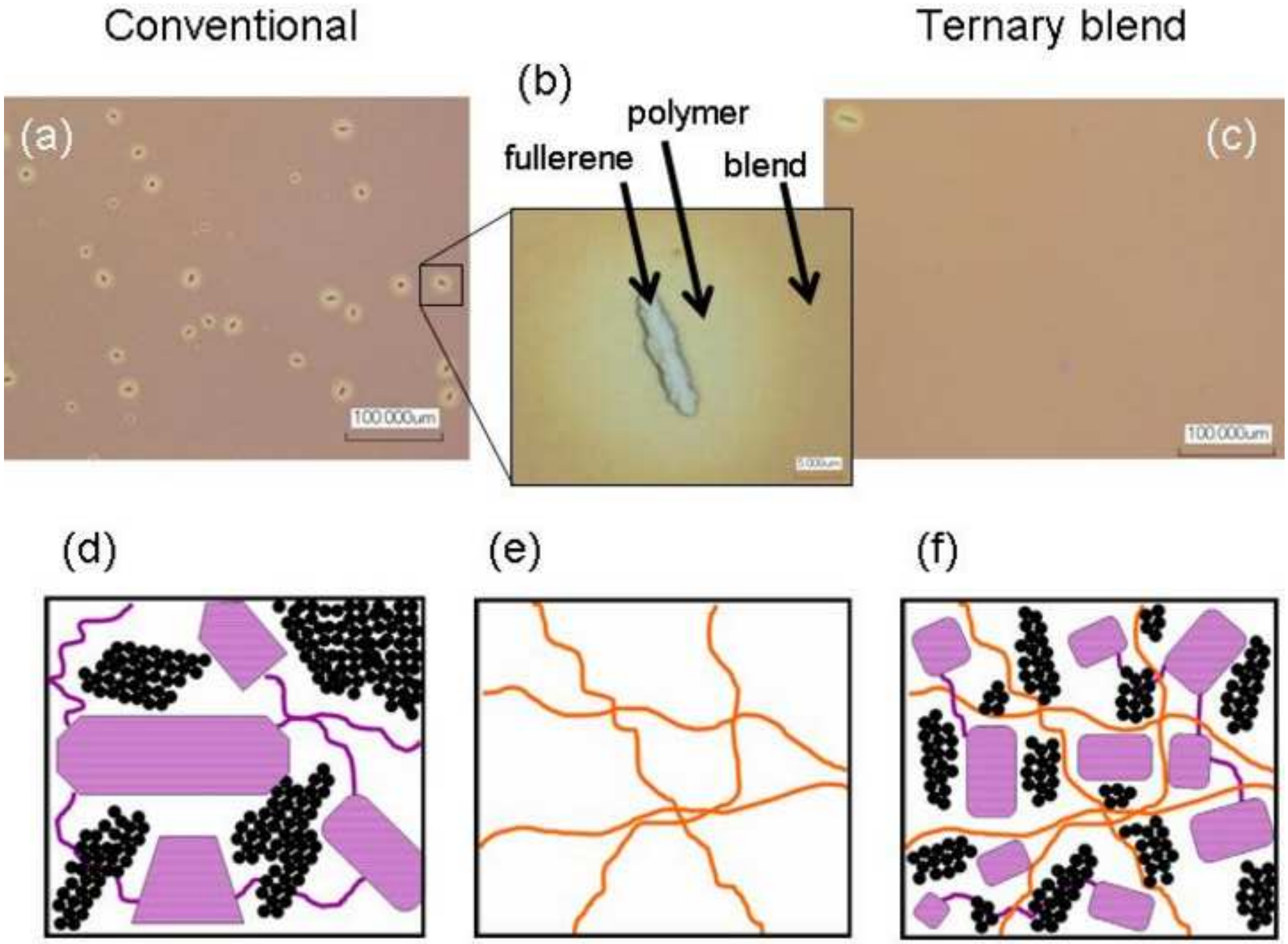
Conventional
Ternary blend
(a)
(b)
(c)
polymer
fullerene
blend
100.000um
100.000um
(d)
(e)
(f)

Figure2

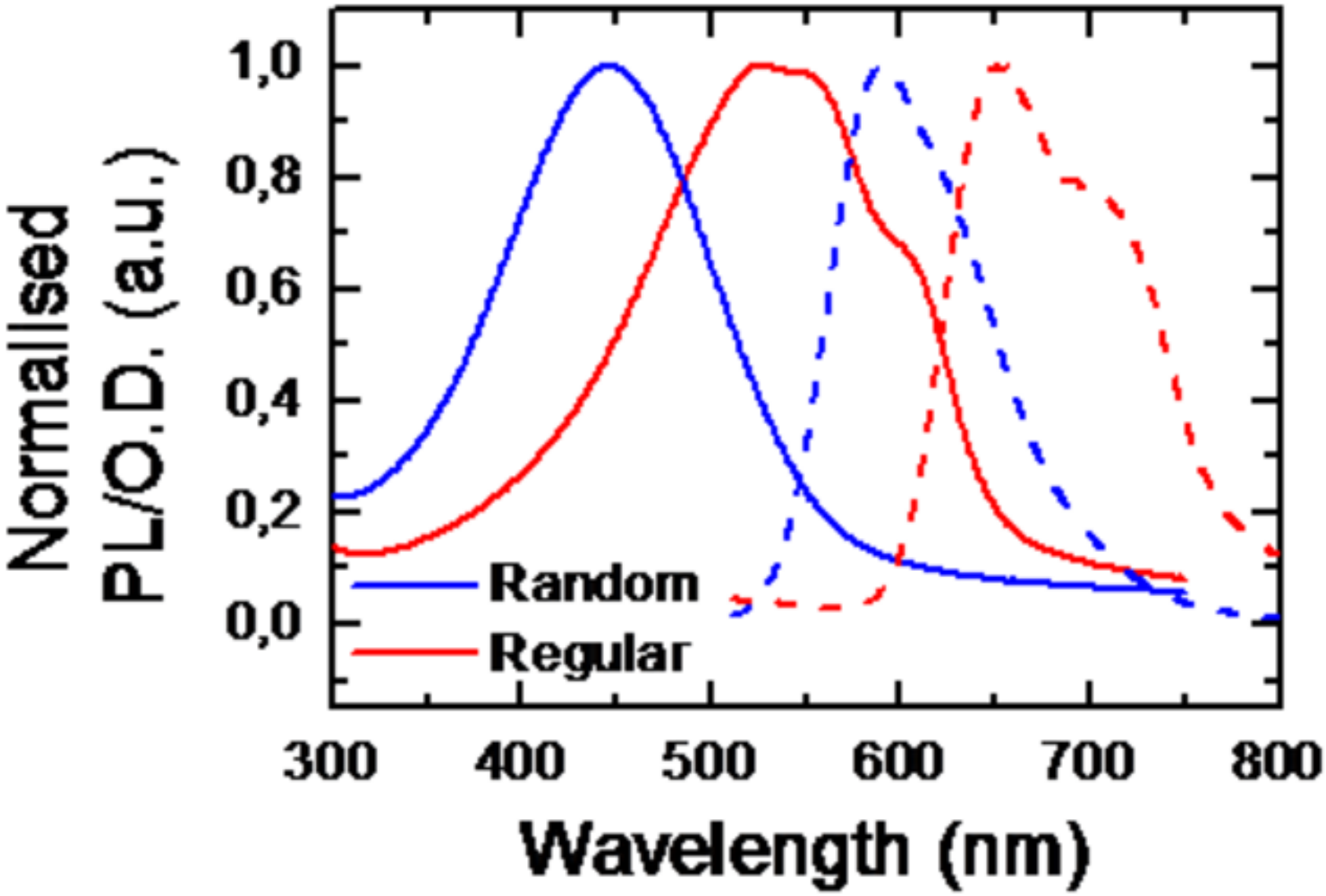
Normallsed
PL/O.D. (a.u.)
1,0
0,8
0,6
0,4
0,2
0,0
Random
Regular
300
400
500
600
700
800
Wavelength (nm)

Figure3

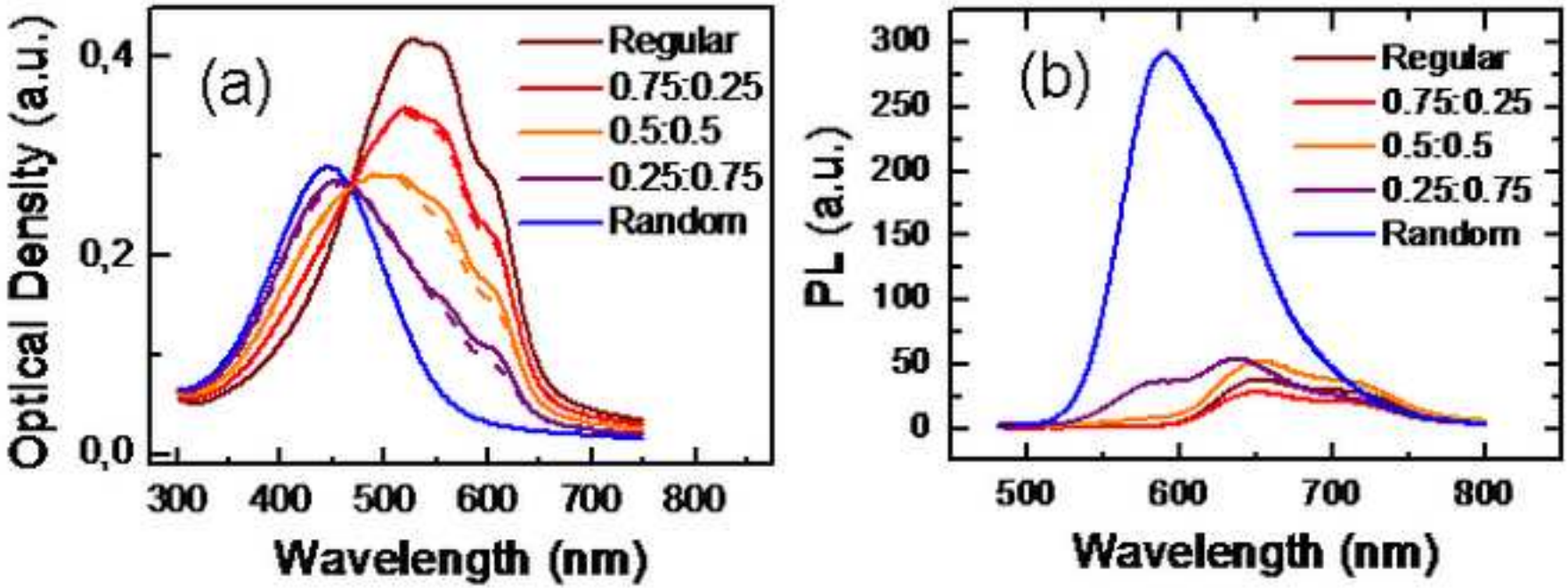
(a)
Optical Density (a.u.)
0,4
0,2
0,0
300
400
500
600
700
800
Wavelength (nm)
Regular
0.75:0.25
0.5:0.5
0.25:0.75
Random
(b)
PL (a.u.)
300
250
200
150
100
50
0
500
600
700
800
Wavelength (nm)
Regular
0.75:0.25
0.5:0.5
0.25:0.75
Random

Figure4

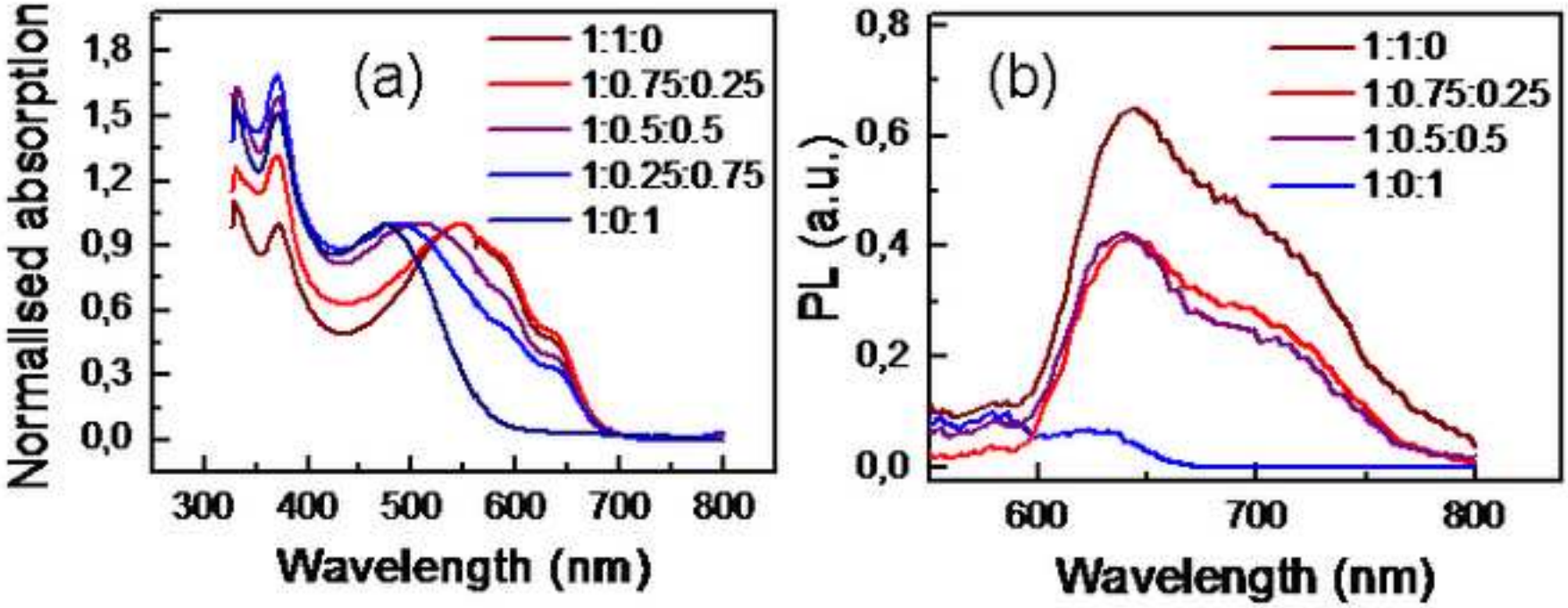
(a)
Normallsed absorption
1,8
1,5
1,2
0,9
0,6
0,3
0,0
300
400
500
600
700
800
Wavelength (nm)
1:1:0
1:0.75:0.25
1:0.5:0.5
1:0.25:0.75
1:0:1
(b)
PL (a.u.)
0,8
0,6
0,4
0,2
0,0
600
700
800
Wavelength (nm)
1:1:0
1:0.75:0.25
1:0.5:0.5
1:0:1

Figure5

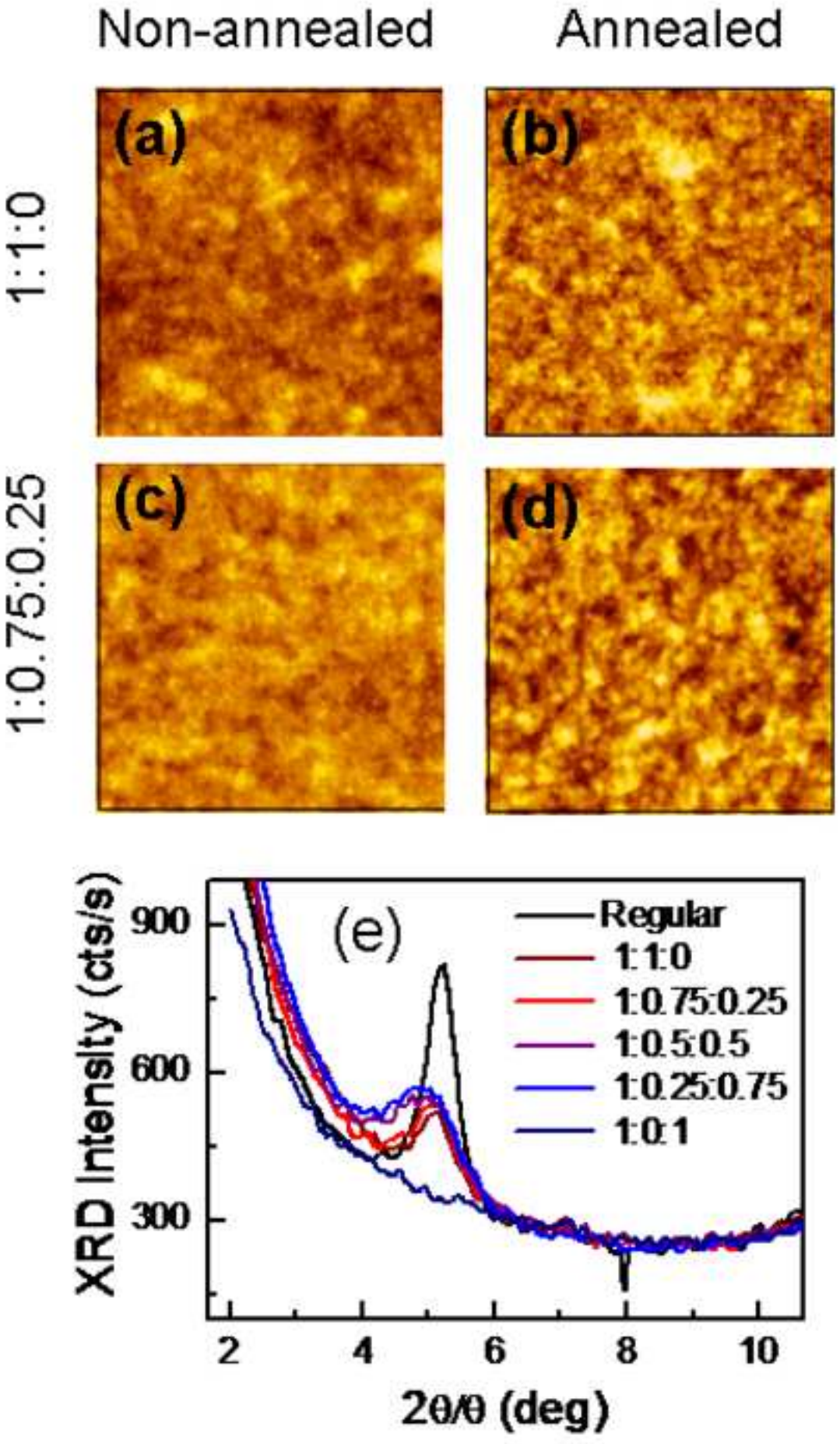
Non-annealed
Annealed
(a)
(b)
(c)
(d)
1:1:0
1:0.75:0.25
(e)
Regular
1:1:0
1:0.75:0.25
1:0.5:0.5
1:0.25:0.75
1:0:1
XRD Intensity (cts/s)
900
600
300
2
4
6
8
10
2θ/θ (deg)

Figure6

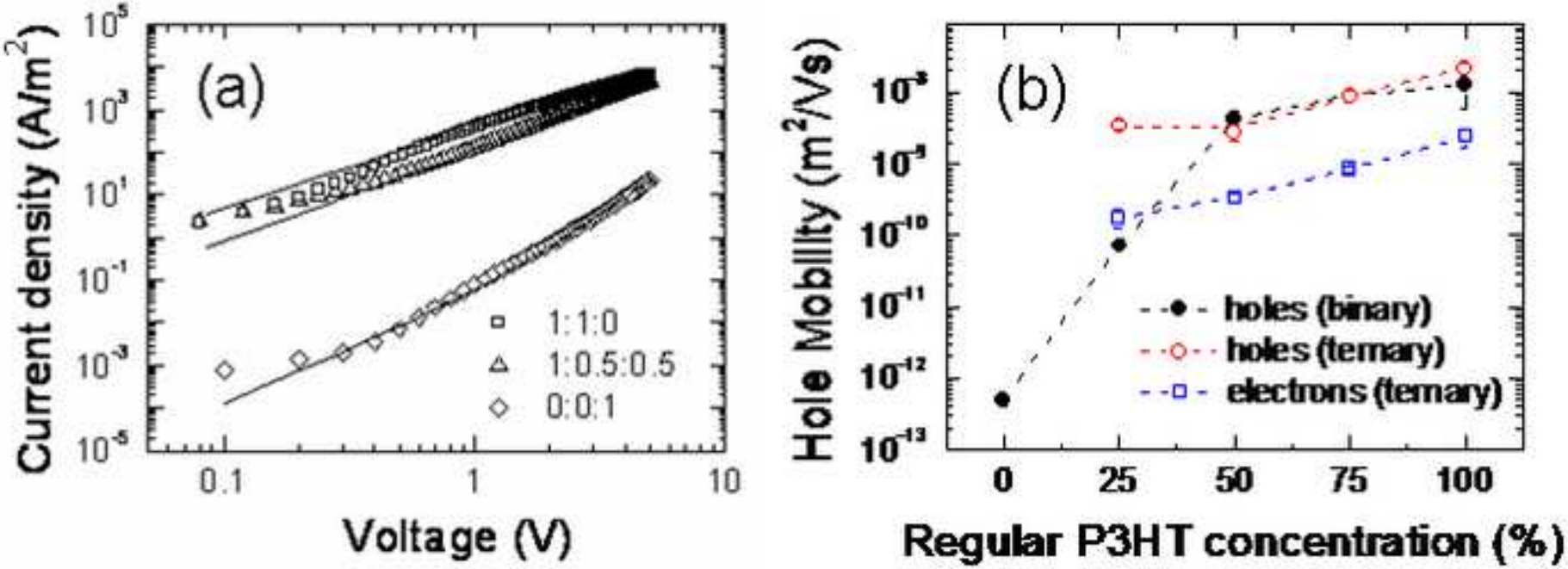
(a)
Current density (A/m$^2$)
Voltage (V)
0.1
1
10
1:1:0
1:0.5:0.5
0:0:1
(b)
Hole Mobility (m$^2$/Vs)
Regular P3HT concentration (%)
0
25
50
75
100
holes (binary)
holes (ternary)
electrons (ternary)

Figure7

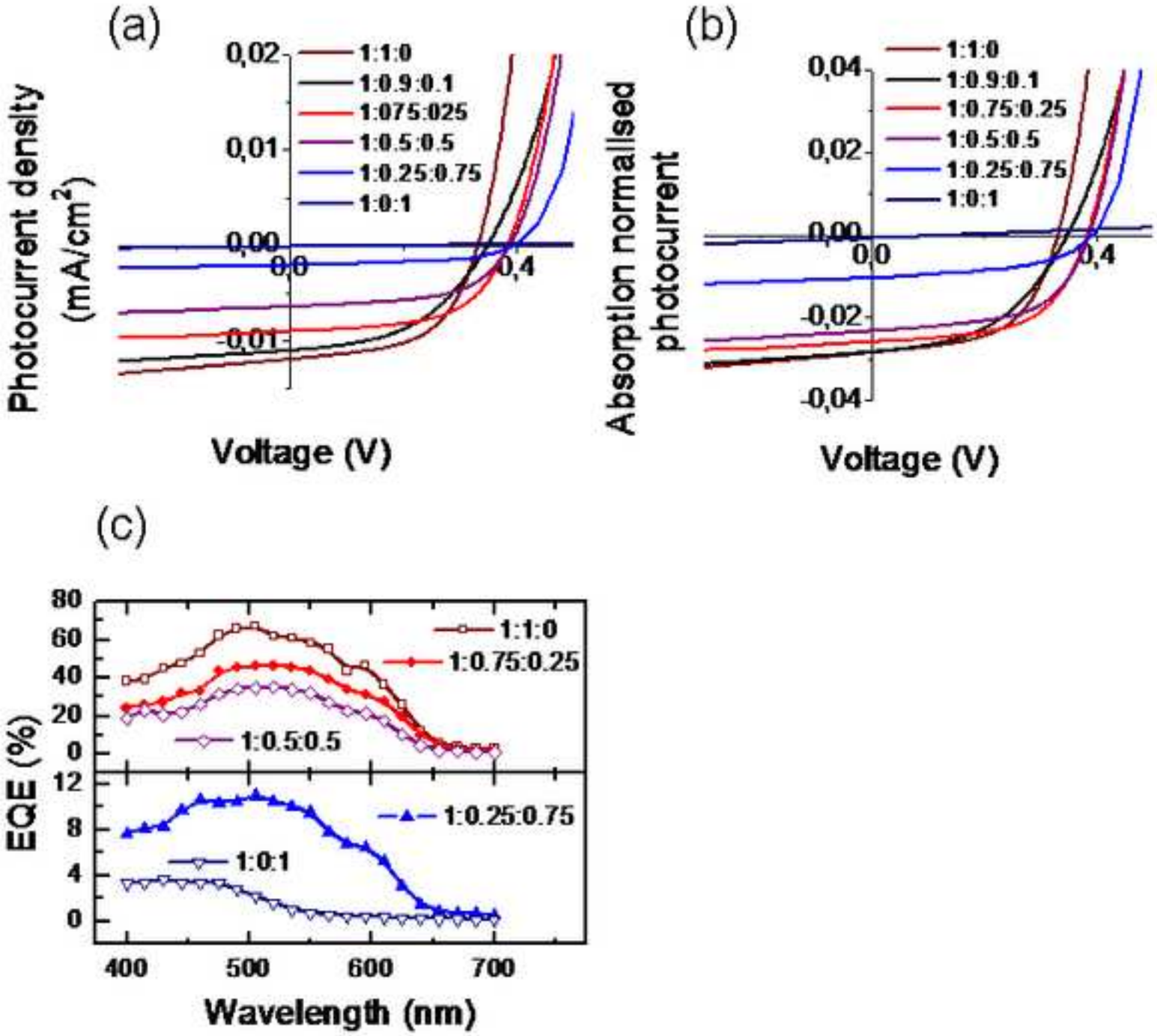
(a)
Photocurrent density (mA/cm²)
Voltage (V)
1:1:0
1:0.9:0.1
1:075:025
1:0.5:0.5
1:0.25:0.75
1:0:1
0,02
0,01
0,00
-0,01
0,0
0,4
(b)
Absorption normalised photocurrent
Voltage (V)
1:1:0
1:0.9:0.1
1:0.75:0.25
1:0.5:0.5
1:0.25:0.75
1:0:1
0,04
0,02
0,00
-0,02
-0,04
0,0
0,4
(c)
EQE (%)
Wavelength (nm)
1:1:0
1:0.75:0.25
1:0.5:0.5
1:0.25:0.75
1:0:1
80
60
40
20
0
12
8
4
0
400
500
600
700

Figure8

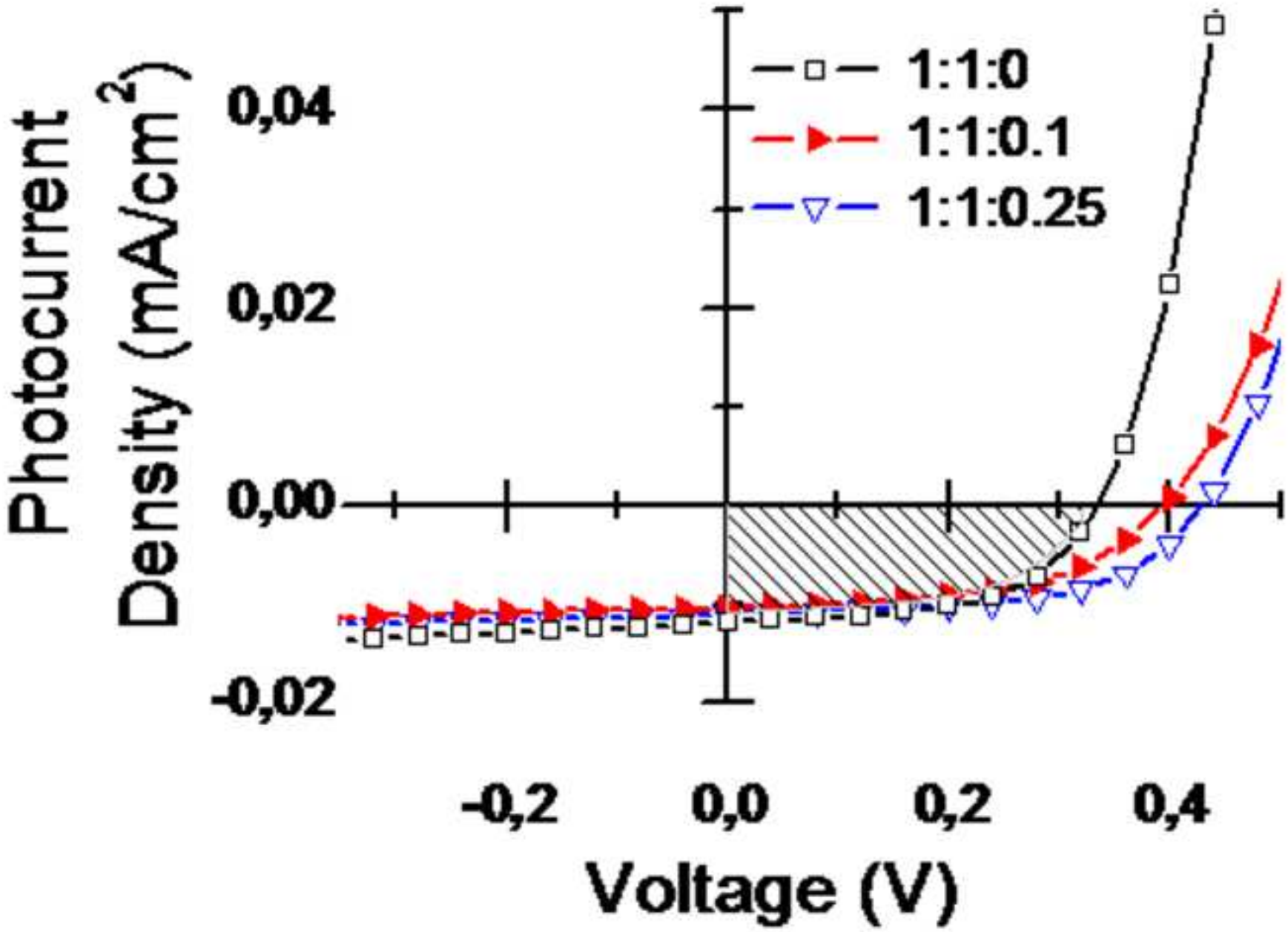
Photocurrent Density (mA/cm$^2$)
0,04
0,02
0,00
-0,02
1:1:0
1:1:0.1
1:1:0.25
-0,2
0,0
0,2
0,4
Voltage (V)

Figure9

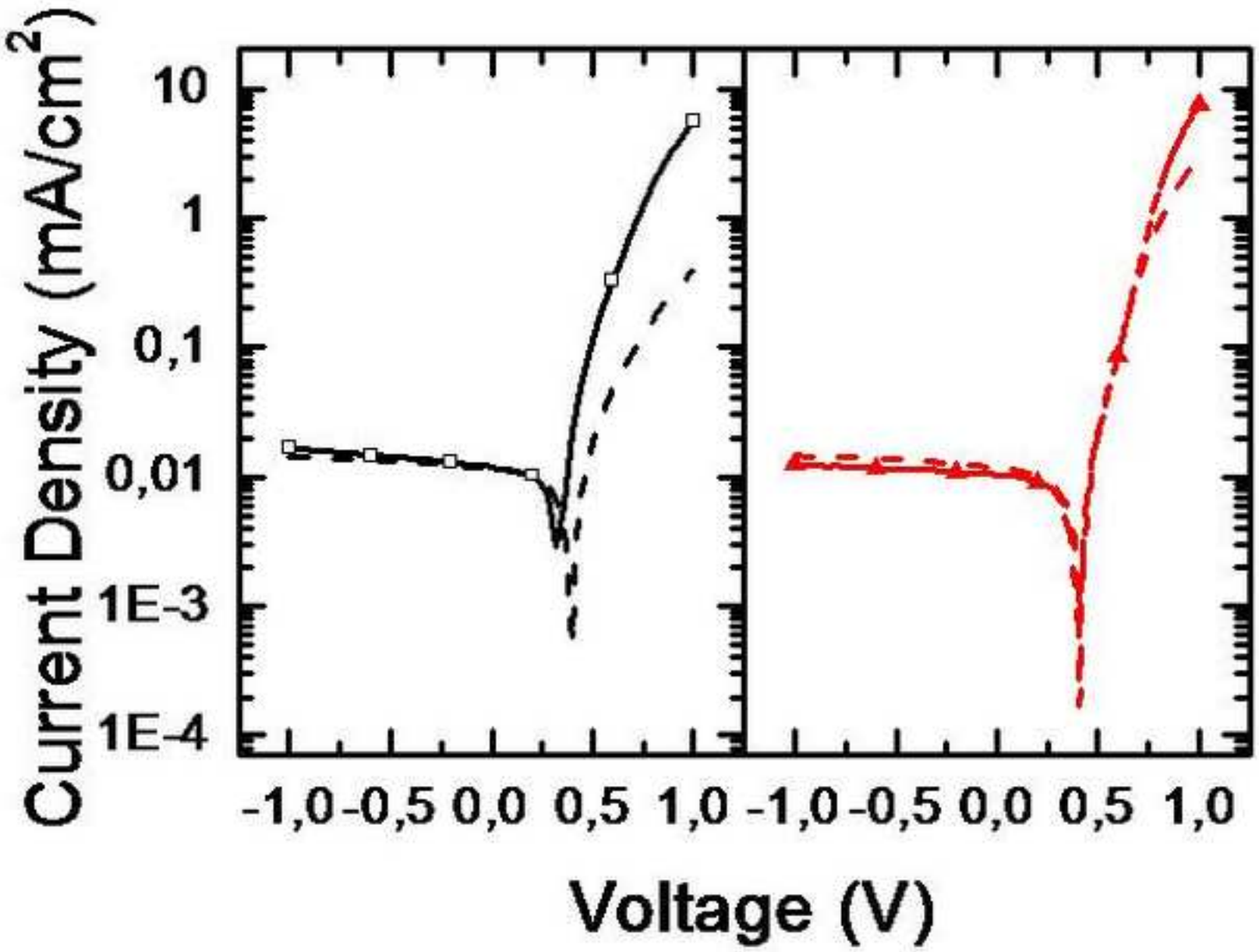
Current Density (mA/cm$^2$)
10
1
0,1
0,01
1E-3
1E-4
-1,0 -0,5 0,0 0,5 1,0 -1,0 -0,5 0,0 0,5 1,0
Voltage (V)

Figure10

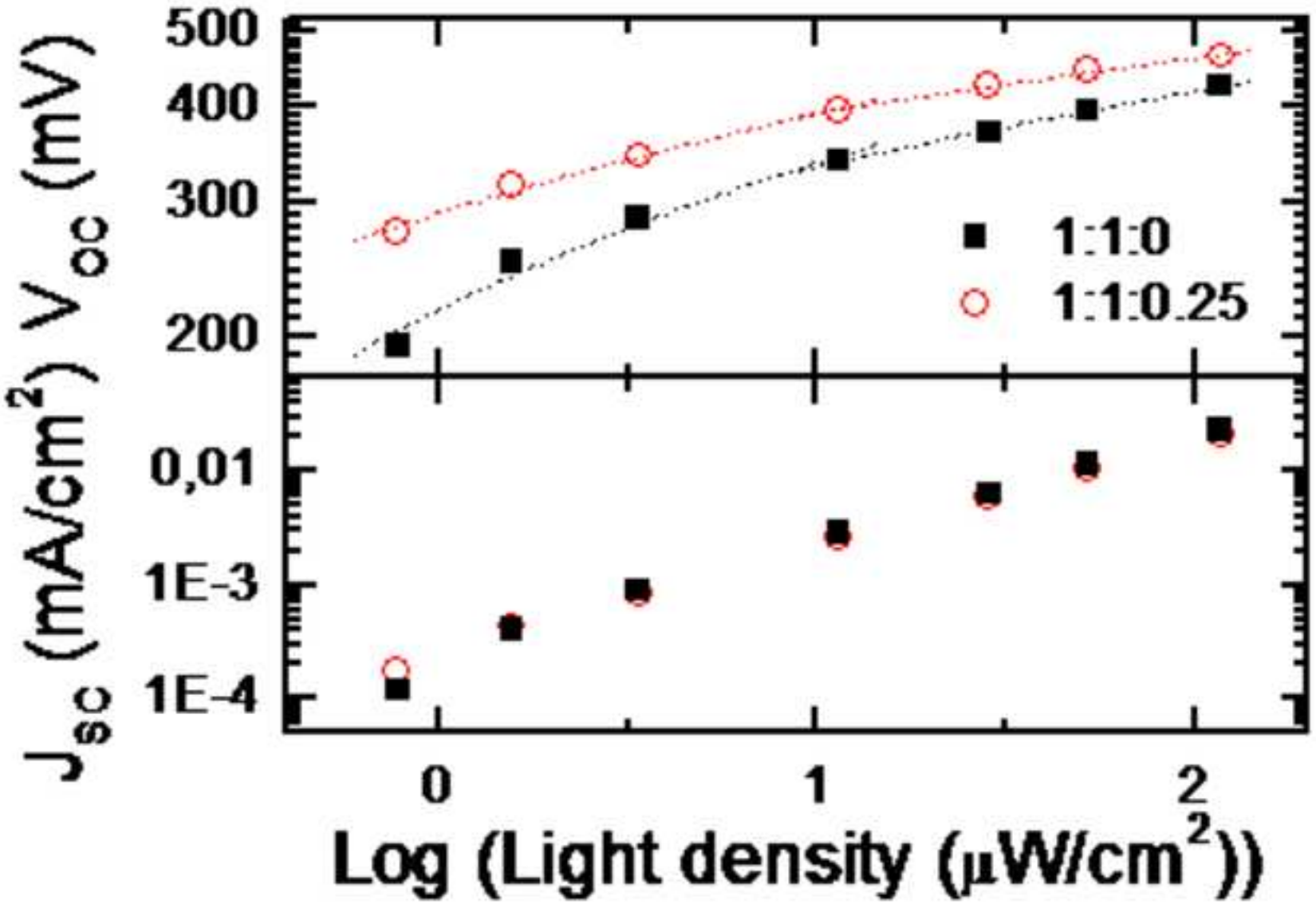
500
400
300
200
0,01
1E-3
1E-4
0
1
2
1:1:0
1:1:0.25
$J_{sc}$ (mA/cm$^2$) $V_{oc}$ (mV)
Log (Light density (μW/cm$^2$))

**Table I**

| | 1:1:0 | 1:0.75:0.25 | 1:0.5:0.5 | 1:0.25:0.75 | 1:0:1 |
|---|---|---|---|---|---|
| Interplane distance [nm] | 1.72 | 1.73 | 1.75 | 1.76 | NA |
| Crystallite size [nm] | 16.2 | 13.7 | 10. 1 | 9.8 | 0 |
| Crystallinity [arb.units] | 657 | 755 | 774 | 728 | 0 |
| Absorption (550nm) | 0.418 | 0.346 | 0.275 | 0.198 | 0.123 |
| lambda max Abs [nm] | 546 | 548 | 512 | 479 | 473 |
| Ra roughness [nm] | 0.7 | 1 | 1.2 | 0.9 | 1 |
| RMS roughness [nm] | 0.9 | 1.3 | 2 | 1.3 | 0.6 |
| Hole mobility [$m^2/Vs$] | 2.20E-08 | 9.12E-09 | 2.76E-09 | 3.48E-09 | - |
| Electron mobility [$m^2/Vs$] | 2.38E-09 | 8.41E-10 | 3.35E-10 | 1.77E-10 | - |
| $J_{sc}$[$mA/cm^2$] (550 nm) | 0.0119 | 0.0090 | 0.0064 | 0.0020 | 0.0001 |
| $J_{sc}$/Abs(550nm) | 0.0285 | 0.0259 | 0.0233 | 0.0102 | 0.0007 |
| 100*$J_{ma}$*$V_{max}$/Abs (550nm) | 0.534 | 0.577 | 0.518 | 0.204 | 0.003 |
| $V_{oc}$ [mV] (550 nm) | 331 | 384 | 390 | 391 | 147 |

**Figure1-Black and white-for print**

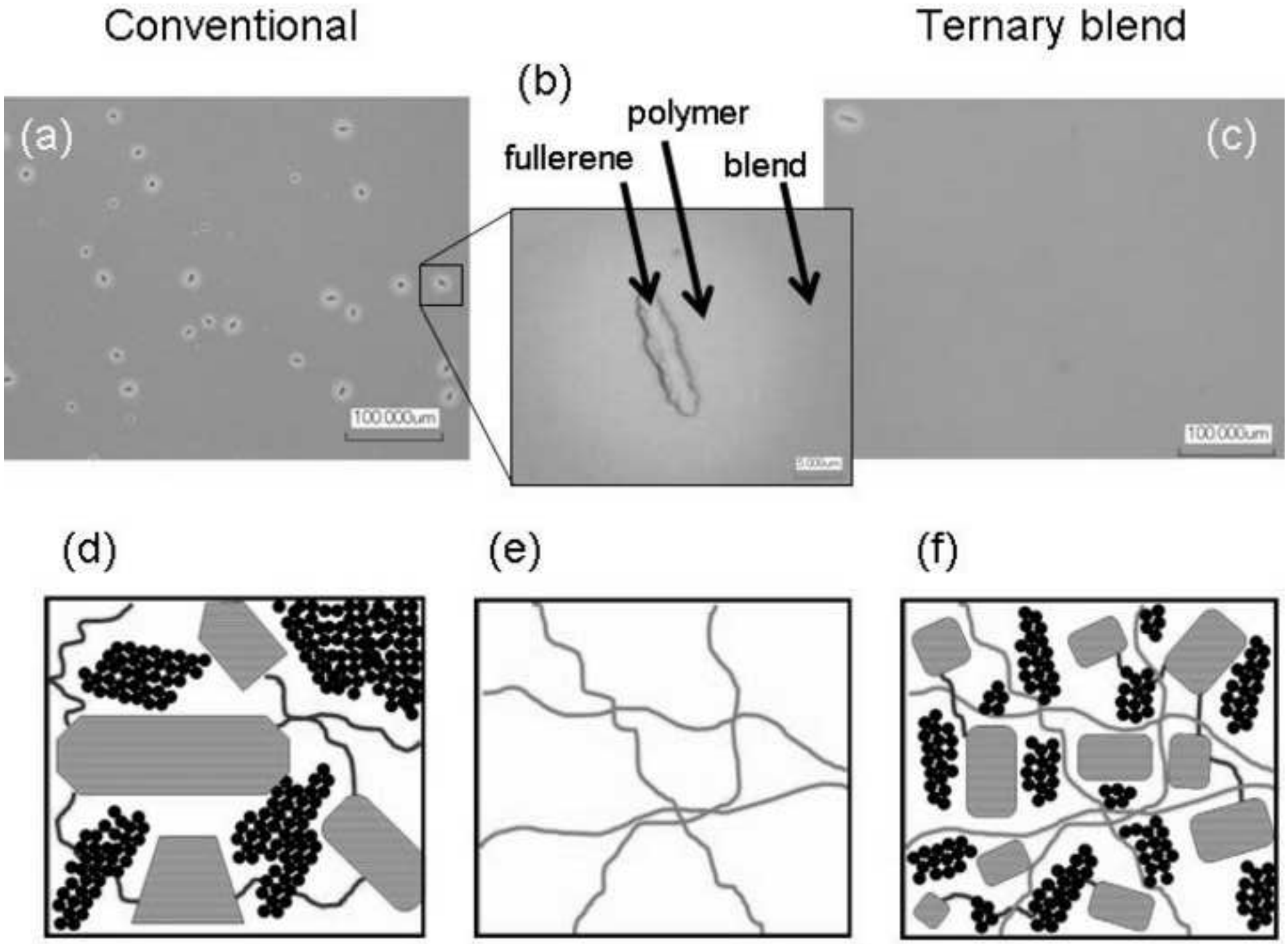

Figure2-Black and white-for print

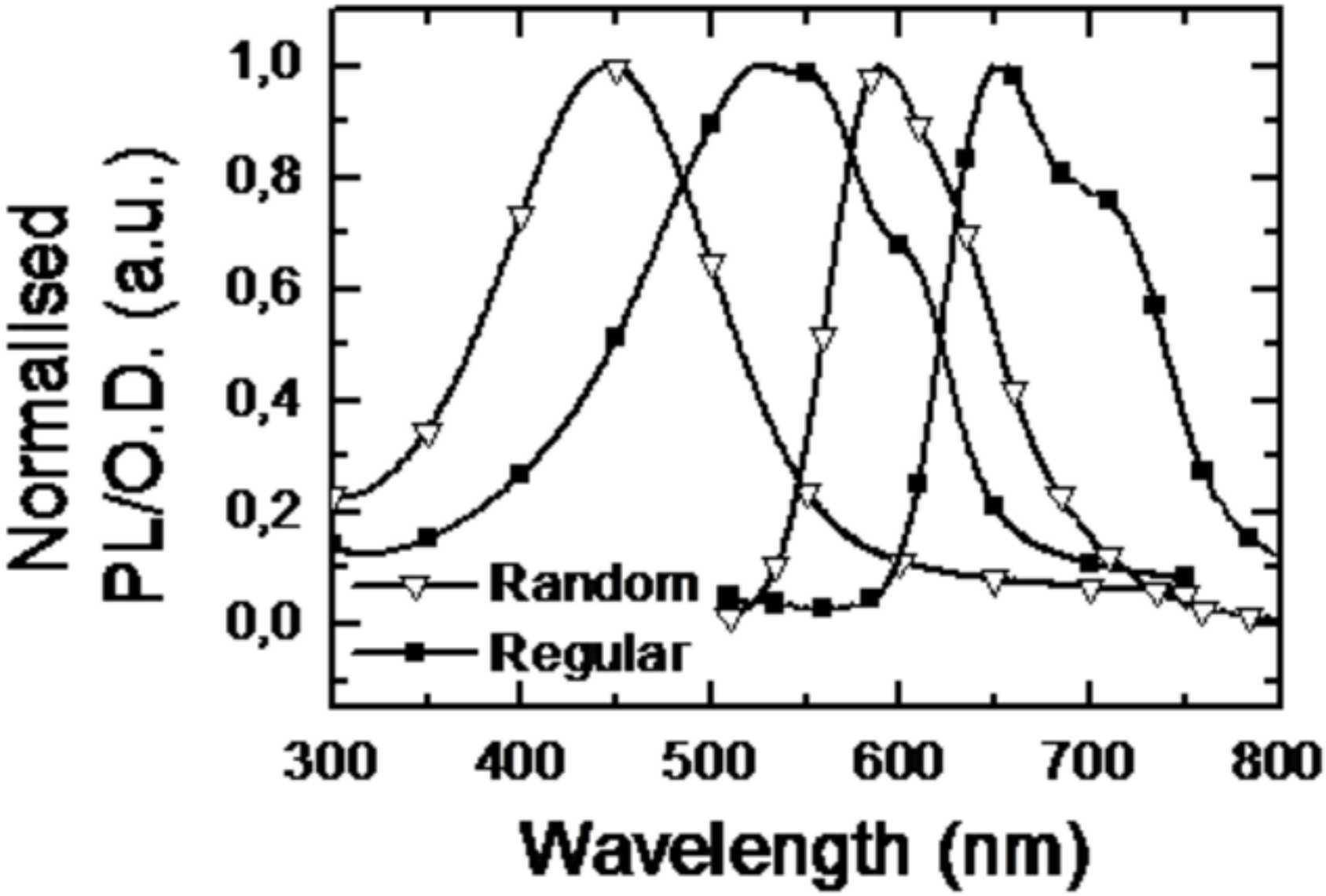

Figure3-Black and white-for print

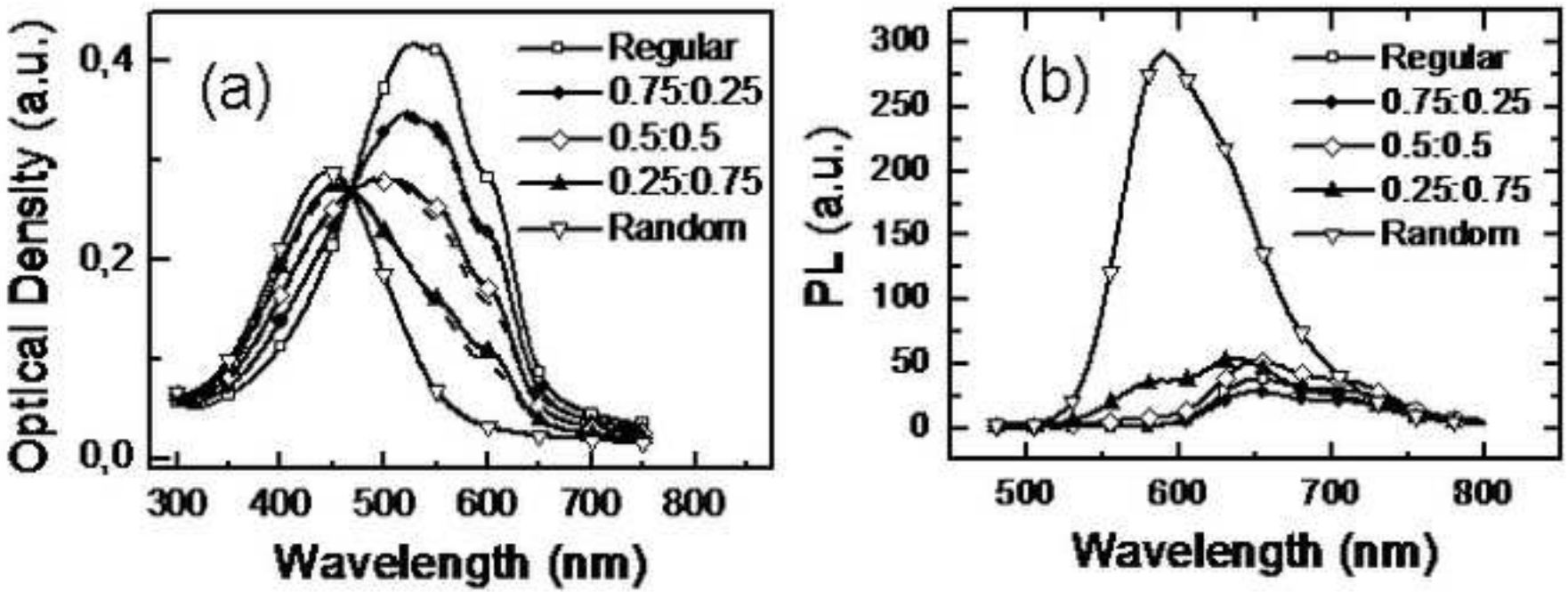

Figure4-Black and white-for print

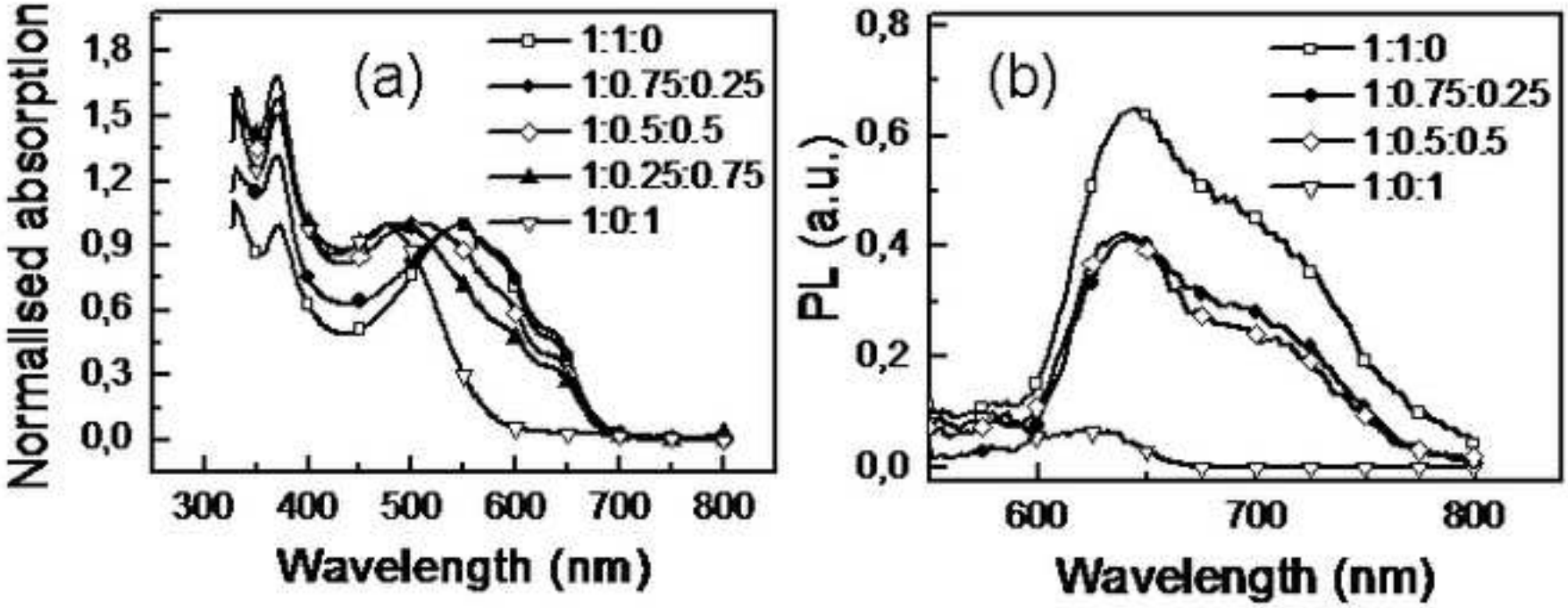

**Figure5-Black and white-for print**

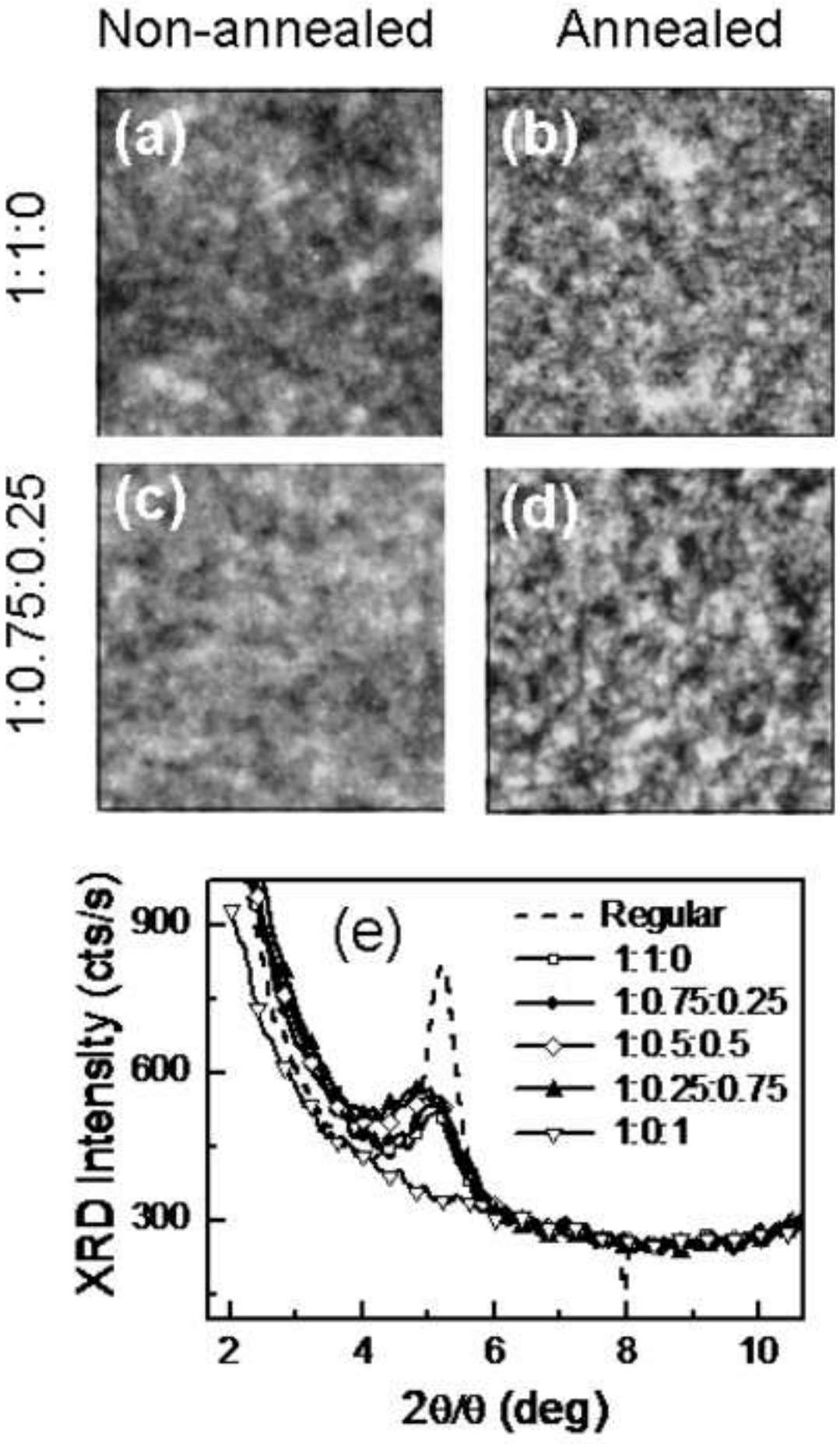

Figure6-Black and white-for print

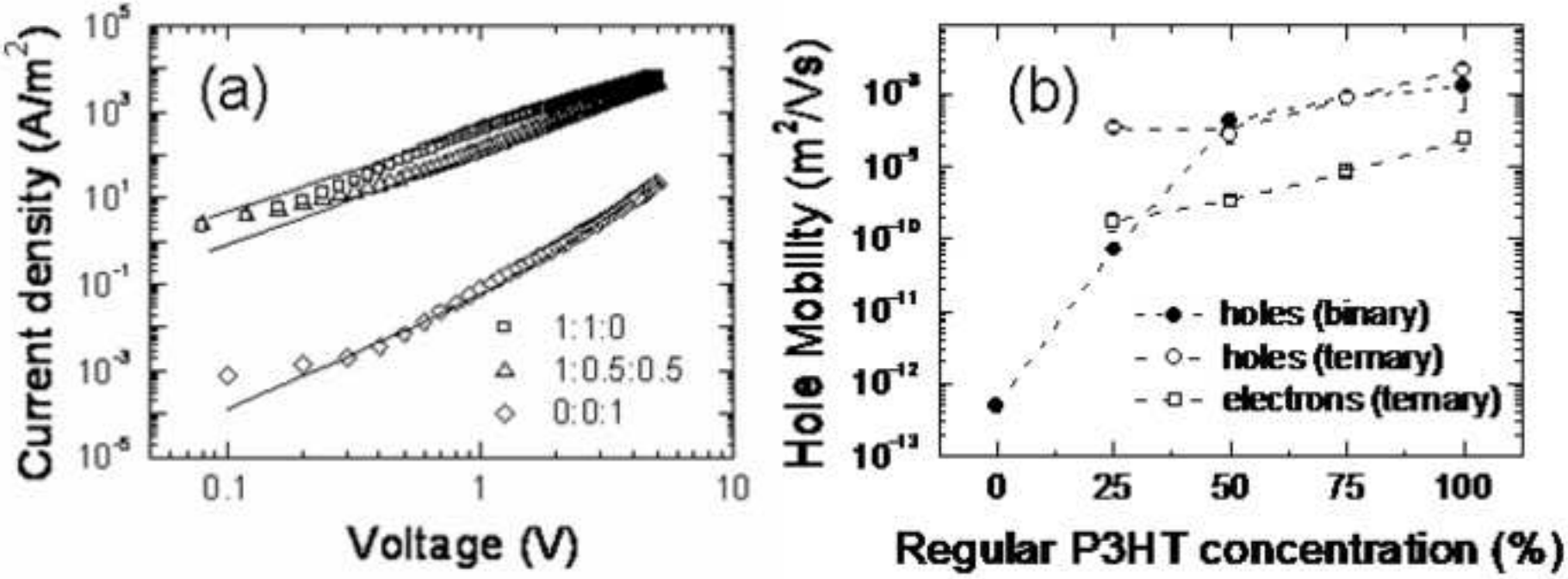

Figure7-Black and white-for print

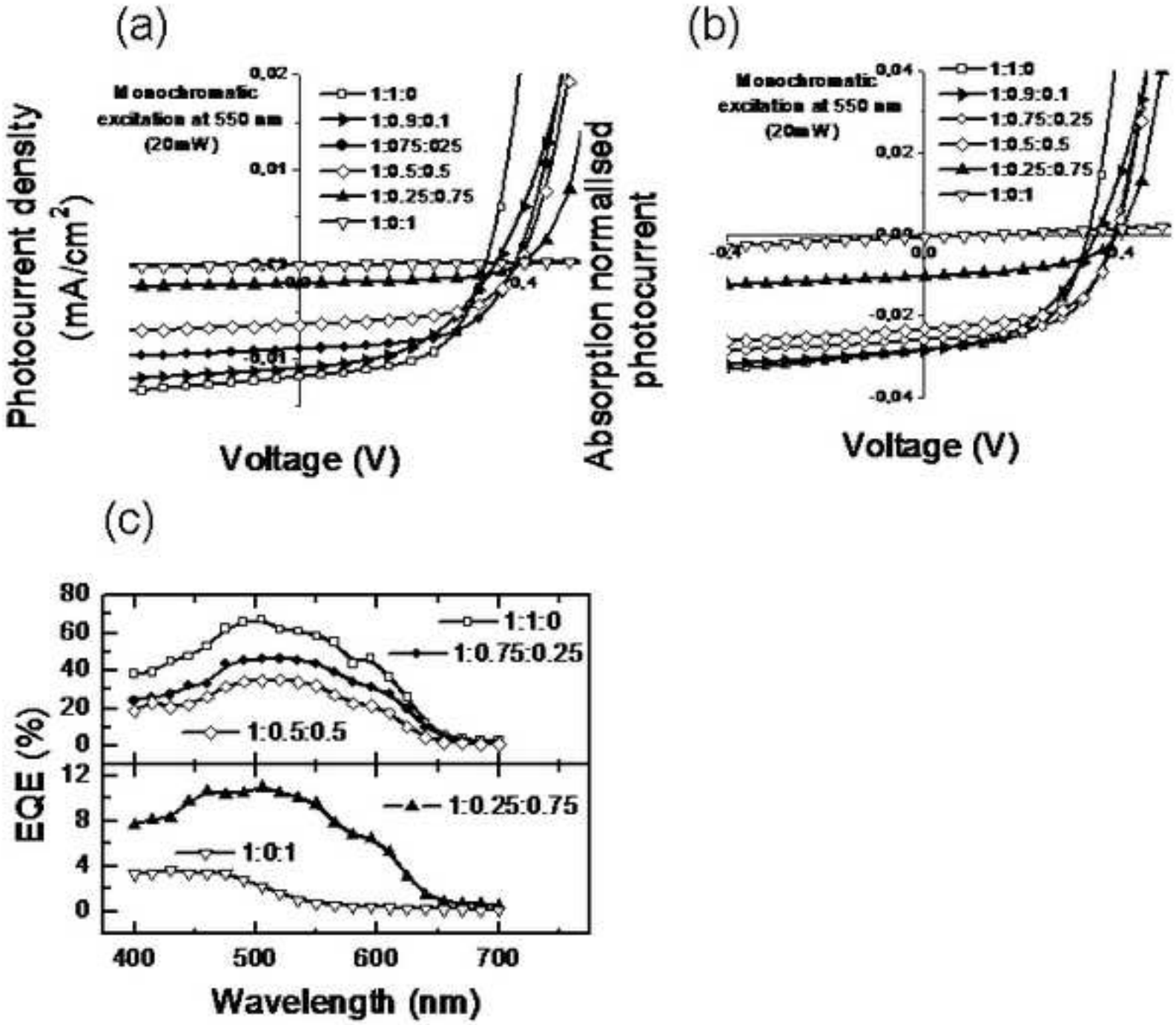

Figure8-Black and white-for print

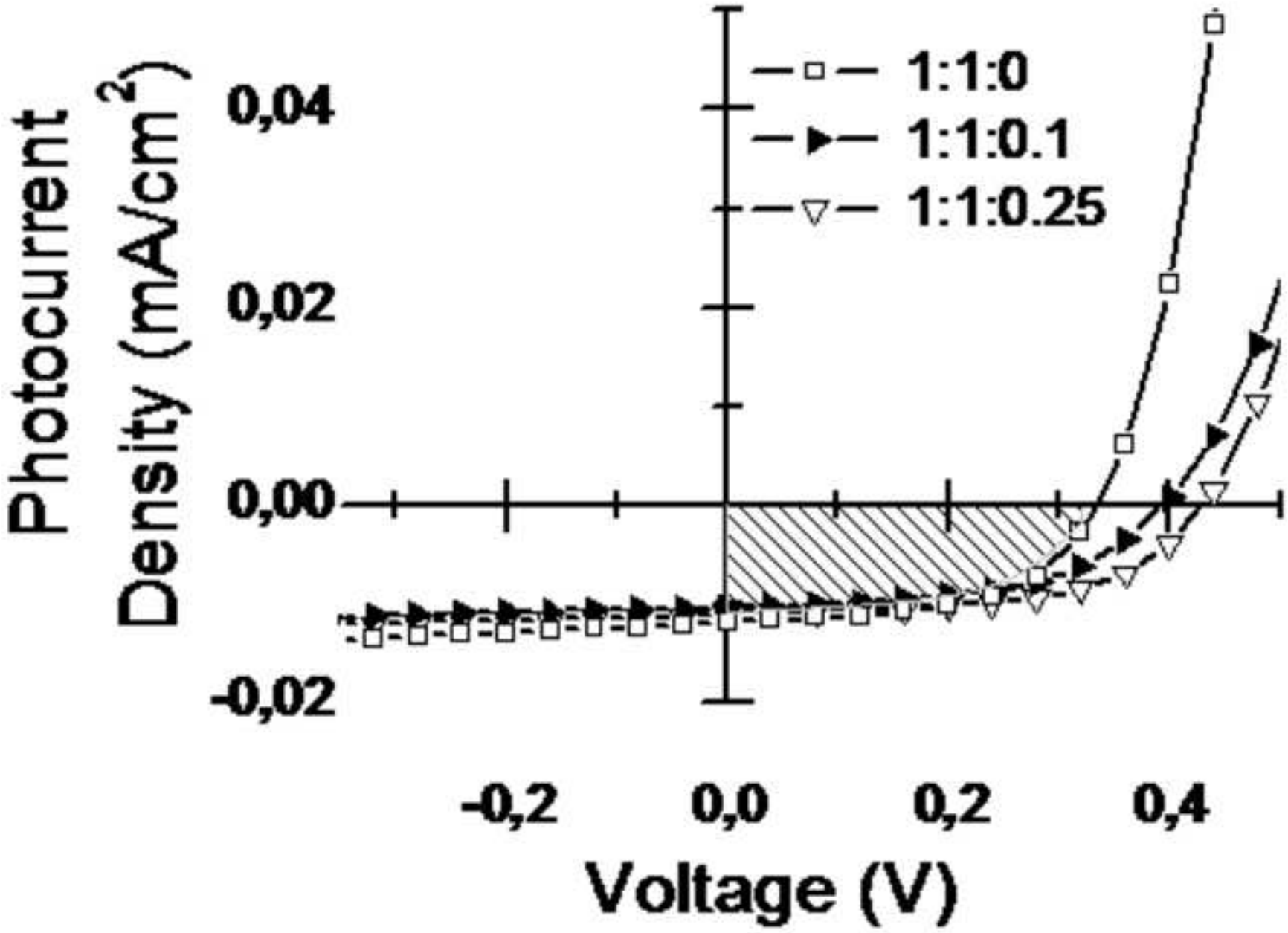

Figure9-Black and white-for print

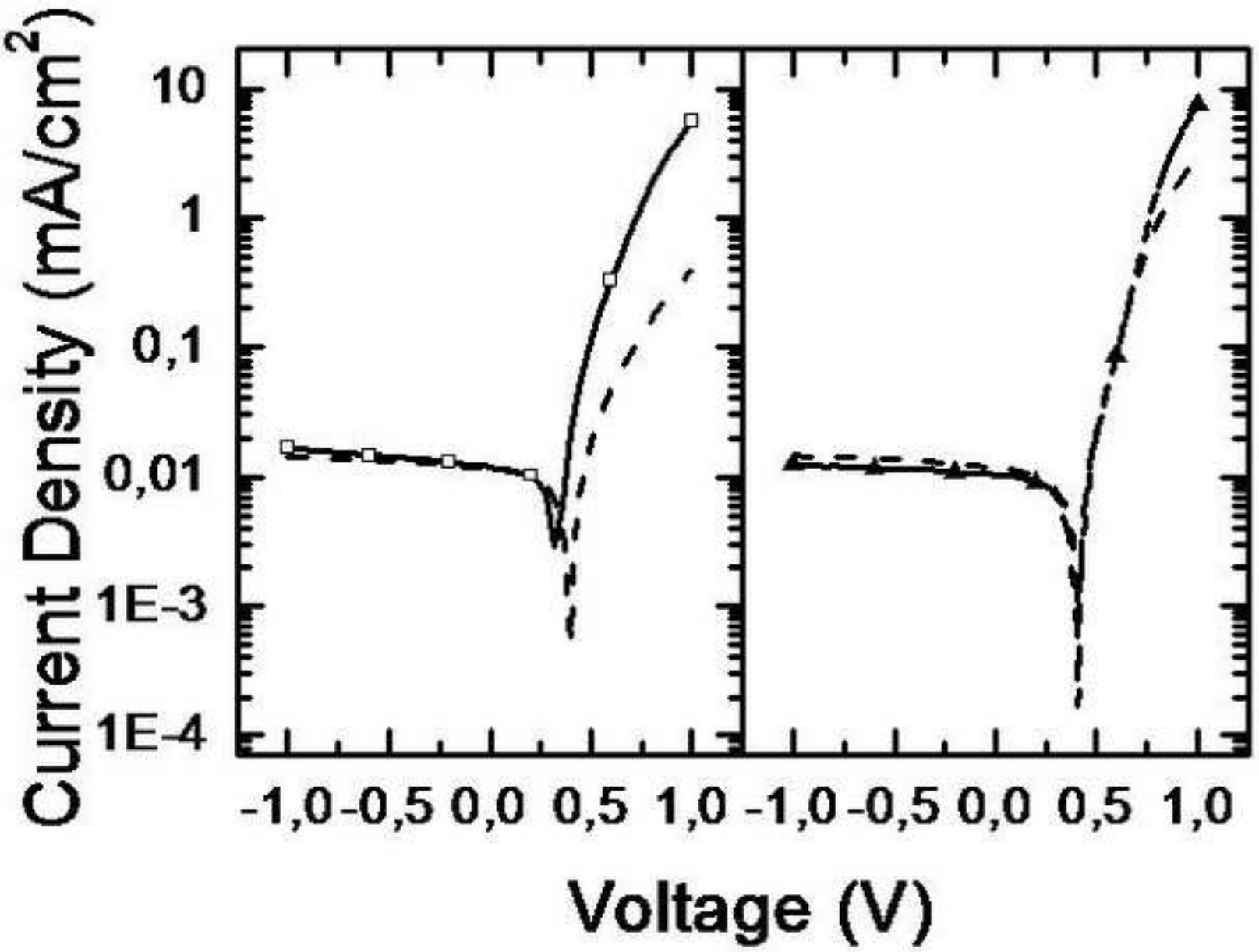
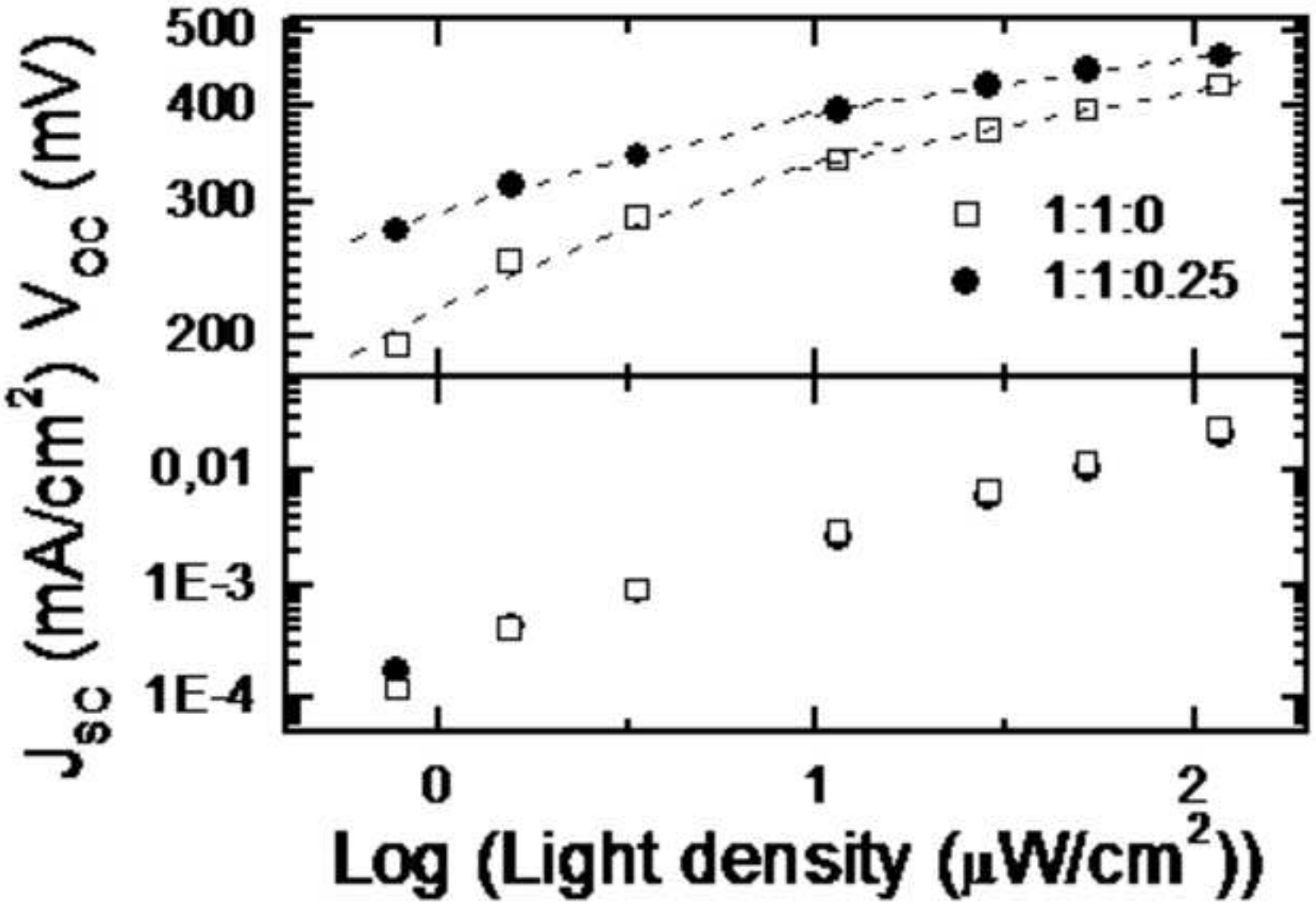
Figure10-Black and white-for print